### RESEARCH ARTICLE



Check for updates

# Importance of higher modes for dynamic soil structure interaction of monopile-supported offshore wind turbines

# Upendra Kumar Sah | Jun Yang 🏻



Department of Civil Engineering, The University of Hong Kong (HKU), Pokfulam, Hong Kong

#### Correspondence

Jun Yang, Department of Civil Engineering, The University of Hong Kong (HKU), Pokfulam, Hong Kong. Email: junyang@hku.hk

#### **Funding information**

Research Grants Council, University Grants Committee

#### **Abstract**

Offshore wind turbines (OWTs) have emerged as one of the most sustainable and renewable sources of energy. The size of OWTs has been increasing, which creates more challenges in the design of foundations due to the potential highermode effects involved in the dynamic soil-structure interaction (DSSI) response. Several foundation modeling techniques are available for calculating the OWT fundamental frequency; however, their capability to predict the higher modes by considering real geometric configurations is unclear. The main aim of this study is to perform a rigorous modal analysis of the NREL 5MW reference OWT to investigate the higher mode effects using the 3D finite element method. A detailed parametric analysis is also performed to study the effects of soil inhomogeneity, initial soil modulus, and the monopile dimensions (diameter, thickness, and embedded pile depth) on higher modes' natural frequencies and effective mass participation ratios. The study shows that dynamic soil-structure interaction has a significant role in modal response and the simplified foundation models are not accurate enough. Given the significant contribution from higher modes, they should not be simply ignored in the OWT design, particularly in earthquake-prone zones.

#### KEYWORDS

dynamic soil-structure interaction, higher mode, offshore wind turbine, simplified model

### INTRODUCTION

Offshore wind energy is becoming a leading renewable energy source as a result of its huge deployment across the world.<sup>1-3</sup> The Global Wind Energy Council (GWEC) report shows rapid growth in the construction of wind farms in earthquakeprone areas such as Europe, Asia-Pacific, and the Americas due to high-energy demand. However, the breakthrough in offshore wind energy development is hampered by the high cost of OWT's foundations. Offshore wind turbines offer a unique, slender structure with a heavy mass located at the top level. The analysis and design of such a structure is a challenge due to different kinds of uncertain cyclic loading (wind, wave, and earthquake load) on top of static gravity loads.<sup>4,5</sup> In the last decade, both the capacity and size of offshore wind turbines have been increasing due to their higher wind energy harnessing capabilities and lower environmental impact.<sup>6,7</sup> This creates even more challenges in the design

This is an open access article under the terms of the Creative Commons Attribution-NonCommercial License, which permits use, distribution and reproduction in any medium, provided the original work is properly cited and is not used for commercial purposes.

© 2024 The Authors. Earthquake Engineering & Structural Dynamics published by John Wiley & Sons Ltd.

of foundations due to the higher-mode effects involved in dynamic response. Dynamic soil-structure interaction (DSSI) of offshore wind turbines (OWT) plays a key role in dynamic response and in optimizing the foundation design. As the DSSI is a complex dynamic phenomenon, its effect might be beneficial or detrimental depending on the type of structure, soil condition, and loading type. Hence, an explicit understanding of the effects of DSSI on the OWT environment is crucial.

The basis for the economical and safe design of structures depends on the accurate prediction of maximum forces and deformations. Moreover, the seismic demand for tall structures like modern offshore wind turbines is influenced by multiple modes of vibration. The research on the effects of higher modes in dynamic response has been mostly focused on conventional infrastructure like high-rise buildings, bridges, tall RC walls, and so forth. II-I5 In order to improve structural and geotechnical analysis, design, and/or assessment, so far, no attention has been paid to offshore wind turbines toward an understanding of higher mode effects. The offshore wind turbine is quite different from conventional structures like tall buildings in terms of mass and stiffness distribution along the height of the structure. In the case of OWT, heavy mass is located on the top of the turbine, whereas in tall buildings, mass is distributed almost uniformly along the height. This makes the seismic demand (base shear, overturning moment, displacement, etc.) and performance different as they mainly depend on the mass and stiffness of the structure. Further, OWT is situated in severe sea environments against extreme natural hazards like earthquakes and typhoons that threaten the reliability of wind turbine performance differently than conventional structures.

In general, the tall structure has a longer fundamental period (short fundamental frequency) than that of short structure that has a shorter fundamental period (long fundamental frequency) value due to an increase in mass and a decrease in stiffness. Ductility refers to the ability of a structure to undergo large deformations without losing its strength and stability. Structures with higher levels of ductility exhibit more energy dissipation capacity during seismic events. The ductile behavior redistributes the forces within the structure, reducing the shear forces at certain levels and increasing shear amplification in other regions. The combination of a longer fundamental period and higher ductility leads to increased shear amplification. The longer period allows the structure to resonate with the longer period ground motions, resulting in larger displacements and accelerations, while the higher ductility enables the structure to absorb and dissipate more seismic energy. This combination amplifies the forces within the structure, particularly at certain levels, leading to higher shear amplification. Flexural yielding of the base tends to elongate the fundamental period and further increase the contribution of higher vibration modes (the so-called "higher-mode effects" in earthquake engineering<sup>11</sup>). The mechanisms retain the higher-mode period in the acceleration-sensitive region of the response spectrum, while the fundamental period is located in the velocity-or even displacement-sensitive region. Hence, the higher modes of vibration pose a challenge due to two major phenomena: first, shear amplification, which has been found to increase with increasing fundamental period and ductility; and second, top acceleration magnification. 12,13 Therefore, understanding higher-mode effects is very important for the seismic design of OWTs.

Almost all modern wind turbines have a range of operating frequencies ( $\mathit{IP}$ ) bounded by upper and lower limit rotor speeds. Based on loading frequency ( $\mathit{f}$ ), rotor frequency range ( $\mathit{IP}$ ), and blade passing frequency ( $\mathit{3P}$ ) for three-blade wind turbines, there are generally three design options considered in OWT design, namely soft-soft design (i.e.,  $\mathit{f} < \mathit{1P}$ ), soft-stiff design (i.e.,  $\mathit{1P} < \mathit{f} < \mathit{3P}$ ), and stiff-stiff design (i.e.,  $\mathit{f} > \mathit{3P}$ ), as shown in Figure 1A,B.<sup>17</sup> As the soft-soft design option is better for very flexible structures like floating offshore wind turbines, it is practically impossible to design the bottom fixed offshore wind turbine, and wave load creates high dynamic amplification. The stiff-stiff design approach looks safe; however, this is an uneconomical design because it requires a massive foundation. Therefore, it is seen that most wind turbine designs are based on a soft-stiff approach, as shown in Figure 1A. Nonetheless, all the design approaches mentioned above are mainly applicable for low megawatt wind turbines, and the governing design load is wind; however, the modern wind turbine is very slender, and its frequency range falls in the high-demand seismic load zone as shown in Figure 1B. Therefore, for the wind turbines intended to be constructed in seismic regions, the governing load would be an earthquake rather than wind and waves.<sup>7</sup> This further brings attention to explicitly understanding the seismic demand, where a significant contribution from higher vibration modes is expected.

The construction of wind turbines is found on different foundation types depending on the depth of water, sea bed condition, and turbine rating; however, more than 80% of offshore wind turbines are constructed on a monopile due to their comparatively easy installation and cost-effectiveness at shallow to moderate water depths (25–40 m).<sup>2,18–21</sup> A large-diameter (3–10 m) monopile is a common choice for the foundation of modern offshore wind turbines, but the widely used approach (p-y curve method), as specified in American Petroleum Institute (API) guidelines<sup>22</sup> or Det Norske Veritas (DNV) guidelines,<sup>23</sup> may not be suitable for such large piles.<sup>24–26</sup> This is because the p-y, t-z, and q-z curves recommended by API or DNV were calibrated against the response of small-diameter (610 mm) slender piles (length-to-diameter ratio of ~34) for offshore oil and gas structures. The behavior of large monopiles is like rigid body rotation and displacement,

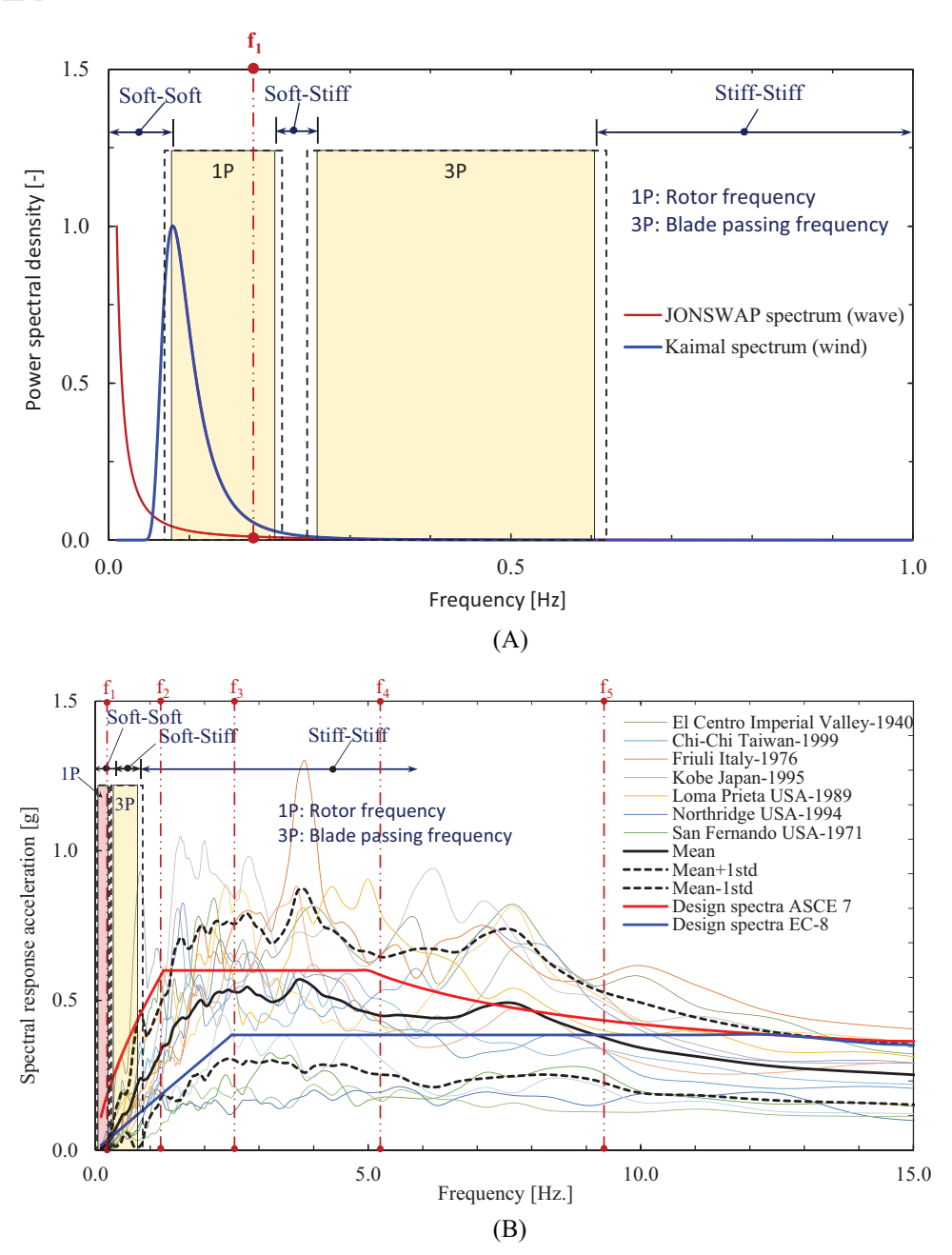


FIGURE 1 (A) Wave and wind spectra along with frequency range of modern wind turbines. (B) Seismic acceleration response spectra along with frequency range of modern wind turbine.

which is different from conventional bending piles.<sup>27</sup> A detailed study with reference to the dynamics of OWTs founded on monopiles is needed.

Two methods (full 3D or simplified) are commonly used to model DSSI problems.<sup>28</sup> The simplified (sub-structure) method is more popular due to its being fast, cost-effective, and requiring less collaboration between structural and geotechnical engineers to implement it.<sup>9,29</sup> Several foundational modeling techniques exist to calculate the OWT fundamental frequency<sup>17</sup>; however, their capability to predict the higher-mode response of large-scale OWTs is unclear. Furthermore, fatigue life is one of the key design criteria for OWT structures. The fatigue damage is due to the wind turbine's inherent frequency approaching the frequencies of cyclic loading (wind, wave, earthquake, 1P, and 3P), which amplifies dynamic demand and causes damage.<sup>30</sup> The method selected for modeling the OWT foundation plays an important role in predicting fatigue damage and structural dynamic response.<sup>8</sup> Therefore, it is necessary to assess and judge the applicability of these DSSI models by considering realistic geometrical configurations for large OWTs, which is one of the purposes of this study. In this regard, the four most popular modeling techniques are considered in this study, namely



**TABLE 1** Properties of five real wind turbines and their foundations.

Wind farm site name											
		wing farr	Irene	Kentish		North	*NREL				
Parameter	Symbol	Lely A2	Vorrink	Flats	Walney 1	Hoyle	5MW	Unit			
Rated Power	P	0.5	0.6	3.0	3.60	2.0	5	MW			
Rotor diameter, Hub diameter	$D_r$ , $D_h$	40.77,1.0	43,1.2	90,2.0	107,2.5	80,1.5	126,3	m, m			
Hub height, Tower height	$H_{h,}$ $H_{t}$	41.5,37.9	51.0,44.5	70.0,60.0	83.5,67.3	70.0,67	90 ,87.6	m, m			
Tower top diameter, wall thickness	$D_{tt,} T_t$	1.9,0.013	1.7,0.013	2.3,0.022	3,0.04	2.3,0.035	3.87,0.019	m, m			
Tower bottom diameter, wall thickness	$D_{tb,} T_b$	3.2,0.013	3.5,0.013	4.45,0.022	5,0.04	4,0.035	6.0,0.027	m, m			
Blade mass, Hub mass, Nacelle Mass	$M_{b,} M_{h,} M_{N}$	6,7,19	7,8,21	31,21,78	44,49,141	24,16,60	53,57,240	tons, tons,			
RNA Lump mass	$M_{RNA}$	32	36	131	235	100	350	tons			
Rotor mass moment of inertia	$I_R$	369	460	9485	19388	5846	33526	tons-m <sup>2</sup>			
Substructure height	$L_{\rm s}$	12.1	6.0	16.0	37.3	7.0	35.0	m			
Monopile embedded depth	L <sub>e</sub>	13.5	19.0	29.5	23.5	33.0	18-60	m			
Monopile diameter	$D_P$ , $Tp$	3.7,0.035	3.5,0.028	4.3,0.045	6,0.08	4,0.05	6.0, 0.06-0.1	m, m			

Note: \*National Renewable Energy Laboratory (NREL): Reference wind turbine.

M1: Full 3D model (reference), M2: Distributed Spring (API 2011<sup>22</sup>), M3: Lump Spring (Gazetas 1991<sup>31</sup>), M4: Improved apparent fixity (Løken et al. 2019<sup>8</sup>), and M5: Fixed at mudline (without SSI effects).

Modal analysis is a powerful technique for identifying the dynamic characteristics of OWTs and gives critical information about modal parameters such as resonant frequency, effective mass participation, mode shape, and damping characteristics of the OWTs. Those characteristics are very important to calculate the dynamic response due to cyclic loads like earthquakes, wind, and waves. This information can help improve reliability and safety at the design stage to prevent an unaccounted failure. Therefore, the main aim of this study is to perform a rigorous modal analysis to get insights into the contribution of higher modes to the dynamic response of OWT systems and further help in the design of new OWTs or the assessment of existing ones. Furthermore, a detailed parametric analysis is performed to study the effects of soil inhomogeneity, initial soil modulus, and the monopile dimensions (diameter, thickness, and embedded pile depth) on the results in terms of system higher mode natural frequency and effective mass participation using the 3D finite element models.

The paper is divided into six different sections, as follows: The Section 1 presents a brief literature review and identifies the research gap as well as the scope of the current research. The Section 2 explains the parameters of OWT and seabed conditions used in this analysis. The Section 3 describes the different types of foundation models and their FEM modeling techniques in 3D Abaqus/Standard. Section 4 briefly introduces the higher mode and modal analysis. Section 5 presents the numerical results of the modal analysis as well as the parametric study, along with a discussion. Finally, some concluding remarks are provided in Section 6.

# 2 | PROPERTIES OF OWT MODEL AND SEABED CONDITION

### 2.1 | Selected offshore wind turbines

Six different offshore wind turbines (Table 1) are chosen for analysis because experimental and numerical data for those structures are available in the literature. The first five real wind turbines are used for verification of the finite element model developed, and the last one (the NREL 5MW OWT) is used for rigorous modal analysis since the information required for the analysis is well documented in previous studies (e.g., Jonkman et al.<sup>35</sup>). It is therefore considered a useful reference model for the analysis of modern OWTs. The five real wind turbines are from different wind farms in Europe,



TABLE 2 Material properties used for the wind turbines.

Part	Material	$\rho$ (kg/m <sup>3</sup> )	E (GPa)	ν
Tower + transition piece	Steel	8500	210	0.3
Monopile in the water Steel	Steel	8880	210	0.3
Monopile in the soil	Steel	7850	210	0.3

*Note*:  $\rho$  = Material density, E = Young's modulus,  $\nu$  = Poisson ratio.

TABLE 3 Soil conditions and input soil parameters used in this study.

		Data ado	pted for thi	s study		
Wind farm name (Country)	Soil condition	$\rho_{\rm s}$ (kg/m <sup>3</sup> )	φ (°)	E <sub>sDp</sub> (MPa)	ν	K <sub>sDp</sub> (MN/m)
Lely A2 (Netherland)	soft clay to dense and very dense sand layer	1800	32	28	0.25	45
Irene Vorrink (Netherland)	Soft silt and clay to dense sand and very dense sand	1800	30	30	0.25	40
Kentish Flats (UK)	Dense sand layer to firm clay	2000	35	70	0.25	77
Walney 1(UK)	Medium and dense sand layers	1900	35	60	0.25	85
North Hoyle (UK)	Clay and Sand layers	1800	32	90	0.25	70
NREL 5MW Reference	Homogeneous and Nonhomogeneous soils	1800	30-40	50-150	0.25	60-125

 $Note: \rho_s = \text{bulk unit weight}, \varphi = \text{Friction angle}, E_{SDp}, K_{SDp} = \text{Initial Young's modulus, initial soil stiffness at one pile diameter}, \nu = \text{Poisson ratio.}$ 

namely Lely A2 (Netherlands), Irene Vorrink (Netherlands), Kentish Flats (UK), Walney 1 (UK), and North Hoyle (UK). The turbine properties as well as the foundation characteristics are collected from the literature<sup>2,10,32–34</sup> and summarized in Table 1.

In general, the effect of power is associated with the size and geometry of the OWT. According to Abo-Khalil et al., <sup>71</sup> the power generated by a wind turbine is directly proportional to the square of the blade length. From a structural and geotechnical point of view, to support the bigger rotor size, it needs a bigger tower height and consequently high gravity loading that alters the dynamic characteristics (natural frequency, mode shape, and effective mass participation) of the system, which demands a bigger foundation size (e.g., diameter, thickness, and embedded depth). As the power-generated capacity of modern wind turbines (>10 MW) is higher than that of past wind turbines, this study also carried out a detailed parametric study that covers a range of monopile dimensions for modern OWT (e.g., monopile diameter, monopile wall thickness, and embedded depth). As for the effect of a larger superstructure for modern wind turbines, it will be studied in the future when the necessary information becomes available. The same methodology can be adopted. It is noticed that both the outer diameter and wall thickness of the tower increase linearly from the tower top to the tower bottom. This study assumes a uniform blade wall thickness of 0.019 m to match the mass of each blade of 17,740 kg, as reported by Jonkman et al. <sup>35</sup> The grade of steel used for the monopile, the tower, and the transition piece is S355 with elastic isotropic behavior. The monopile density used in the analysis is 7850 kg/m³, whereas the density of the tower is taken as 8500 kg/m³ because there is no direct consideration for the paint, welds, bolts, and flanges in the numerical model. The Young's modulus of steel is taken as 210 GPa for all parts, <sup>8,17,35</sup> as shown in Table 2.

# 2.2 | Selected seabed conditions

The soil data reported in the literature for five different wind farms in Europe, namely Lely A2 (Netherlands), Irene Vorrink (Netherlands), Kentish Flats (UK), Walney 1 (UK), and North Hoyle (UK), are available in a descriptive way only, which is not sufficient for analysis; numerical data need to be assumed. The numerical data used in this study for those sites were collected from various literatures 31,34,36,37 and reported in Table 3. The basic types of soil found in offshore site circumstances are cohesive soils, cohesionless soils, and weathered bedrock. In order to cover the wide range of soil conditions at the OWT site, three common soil profiles based on Young's modulus and strength distributions over the depth (Figure 2), namely uniform (homogeneous), linear (inhomogeneous), and parabolic (inhomogeneous), are investigated in this study. They represent (a) an over-consolidated clay whose undrained shear strength and Young's modulus are roughly constant with depth, (b) a normally consolidated clay whose undrained shear strength and Young's modulus

Note: Le is embedded length, Le is critical length

FIGURE 2 Idealization of soil stiffness variation for offshore wind turbine (OWT).

increase linearly with depth, and (c) a sandy soil site whose Young's modulus increases parabolically at the moderate strain level, respectively. In Figure 2,  $E_{so}$  and  $E_{sDp}$  denote Young's modulus at the soil surface (z = 0) and at the depth of one pile diameter, respectively ( $z = D_p$ ).

The detailed analysis of the NREL 5MW offshore wind turbine is carried out using homogeneous and non-homogeneous sands. For the modal analysis, the initial tangent (small-strain,  $<10^{-3}$ ) shear modulus ( $G_{max}$ ) or Young's modulus ( $E_{max}$ ) is required at different depths of soil. There are many empirical equations to evaluate the value of the  $G_{max}$  (kPa) profile, which depends on soil properties (vertical effective stress, relative density, or initial void ratio). <sup>38–41</sup> However, in this study, the equations mentioned in DNV guidelines are used, which depend on the soil properties (vertical effective stress, relative density, or initial void ratio):

$$G_{max} = 22 * (0.6D_r + 16) * \sqrt{\sigma'_m * P_{atm}}$$
 (1)

where  $D_{\rm r}$  is the relative density of sand in %,  $\sigma'_m$  is mean effective stress(kPa),  $P_{\rm atm}$  is atmospheric pressure (kPa)

The small-strain Young's modulus ( $E_{\rm max}$ ) profile in the cases of loose, medium dense, and very dense sands having respectively a relative density ( $D_{\rm r}$ ) of 15%, 35%, and 85% is given in API guidelines, <sup>22</sup> as are the corresponding internal friction angles ( $\phi$ ) 30°, 35°, and 40°; initial void ratios ( $e_{\rm o}$ ) of 0.88, 0.75, and 0.65 are used. <sup>43</sup> The Young's modulus of sand at the depth of one pile diameter ( $E_{\rm SDp}$ ) is tabulated in Table 3.

### 3 | FEM MODEL OF OWT

The detailed three-dimensional (3D) numerical models are developed using the finite element code Abaqus,<sup>44</sup> and the implicit integration scheme is adopted. To ensure the accuracy of the analysis, finite element modeling includes two parts: modeling the superstructure and modeling the dynamic soil-structure interaction. A description of the modeling concept is presented in the following section with the help of Figure 3.

FIGURE 3 Physical representation of offshore wind turbine (OWT).

# 3.1 | Modeling of superstructure

The monopile above the mudline, transition piece, tower, and rotor-nacelle assembly (RNA) together are called the superstructure. The monopile, transition piece, and tower are modeled using C3D20R, a 20-node quadratic brick with a reduced integration element. Many researchers have investigated the modeling issues of the blade, hub, and nacelle. Zuo et al. 45 modeled the blade with full 3D shell elements to consider the influence of aerodynamic behavior. Moreover, Ali et al. 46 have studied the effects of the rotary inertial of blades, rotor eccentricity, blade flexibility, location of failure modes, and seismic vulnerability of OWT towers by considering five different cases. The result showed that the case where  $M_{RNA}$ (total mass of rotor, nacelle assembly) is lumped at the top of the tower by neglecting the rotary inertia of the blade does not capture the seismic vulnerability of wind turbines. However, it is quite accurate to lump the nacelle mass  $(m_N)$  at the nacelle center and the rotor mass (m<sub>R</sub>) at the hub center, along with a vertical and horizontal eccentricity from the tower top, whereas the rotary blade inertial  $(I_R)$  is calculated separately based on blade cross-section and length and applied at  $m_R$ . Similar treatment has been done by other scholars 47,48 as well. As the purpose of this study is to show the effects of the higher bending modes of the tower from the dynamic soil-structure interaction (DSSI) point of view, it is fair enough to lump the blade mass  $(3m_b)$  and rotating moment of inertia  $(I_R)$  at the center of the hub (Hub-CM) together with the hub mass  $(m_H)$  and lump the nacelle mass at the nacelle mass center (Nacelle-CM), as shown in Figure 3. The Hub-CM is eccentric to the tower by an amount of horizontal distance  $(ex_H)$  and vertical distance  $(ez_H)$ , whereas the Nacelle-CM is eccentric to the tower by an amount of horizontal distance  $(ex_N)$  and vertical distance  $(ez_N)$ , as shown in Figure 3. Equation 2 is used to determine the value of  $I_R$ . It is derived by assuming a uniform mass distribution on a thin triangular plate of length  $(r_B)$  to represent the blade and a thin hollow hemisphere of radius  $(r_H)$  to represent the hub.

$$I_R = \begin{cases} I_{xx} \cong 0.5 \ m_B r_B^2 + (2/3) \ m_H r_H^2 \\ I_{yy} \cong I_{zz} \cong 0.25 \ m_B r_B^2 \end{cases}$$
 (2)

where  $m_B$  is blade mass,  $r_B$  is blade length,  $m_H$  is hub mass, and  $r_H$  is hub radius.

The connection between the pile, transition piece, and tower is modeled with the help of the surface-to-surface tie constraints option. The connection between the Nacelle mass center (*Nacelle CM*), Hub mass center (*Hub CM*), and tower top is employed with the help of rigid body constraints tools, where the center of the cross-section at the top of the tower is chosen as a rigid body reference node for both translational and rotational degrees of freedom. In reality, the connection between the monopile pile and tower is stabilized with the help of the transition piece, grouting, and nut-bolt. However, in this study, the flexibilities of the grouted connection between the monopole overhang and transition piece are neglected as they show minor effects.<sup>17</sup> It is assumed that the top diameter of the transition piece is the same as the bottom diameter of the tower, and the bottom diameter of the transition piece is the same as the top diameter of the monopile. The thickness of the transition piece is considered the same as that of the monopile.

# 3.2 | Dynamic soil structure interaction models

For bottom-mounted OWTs, dynamic soil-structure interaction (DSSI) plays a crucial role in the dynamic response. The foundation should be designed to accomplish the interaction between different types of cyclic loading (wind load, wave load, current load, 1P and 3P frequency loads) on top of the rotor-nacelle assembly weight, turbine weight, and the special seabed soil condition at a particular site. The monopile is the most common foundation used, even in modern offshore wind turbines. Its soil-structure interaction modeling techniques have been reviewed by many scholars and extensively used for the analysis and design of OWTs. 17,25,46,49-53 Although different modeling techniques require different input parameters, the determination of parameters for each model is based on the procedures widely accepted in engineering practice to represent the same physical problem. Therefore, the common goal of each model is the same. However, modeling the foundation to capture the explicit DSSI response is still unclear in the literature due to a lack of experimental verification and validation. The existing foundation modeling techniques are only verified for fundamental frequency. The capability to predict the higher-mode response by considering real geometric configurations of OWT is unknown. This study systematically examines the higher-mode frequencies and corresponding effective mass participations using the five most popular modeling techniques, namely the full 3D model (M1); distributed spring (M2); lump spring (M3); improved apparent fixity (M4), and fixed at the mudline (M5), as shown in Figure 4. For all these models, the same superstructure model is adopted.

Inertial mass, stiffness, and damping are the three key factors for modeling water-pile or soil-pile interactions. A continuum model of the structure and its surroundings (soil or water) can provide a comprehensive solution to the interaction problem. Many researchers just take stiffness and damping into account in the simplified model to evaluate the water-pile interaction or the soil-pile interaction since these properties of the surrounding material (water or soil) play a major role in the interaction problem. However, for a more precise response in the simplified model, the inertial force of the surrounding material needs to be involved as well. In this study, the inertial loading of surrounding water for water-pile interaction and soil for soil-pile interaction is modeled approximately by adding the mass as per Equations 3 and 4, respectively.<sup>17,46,48,54</sup> Those two equations are basically derived from the concept of how much mass of the surrounding material (soil or water) is displaced. The displaced mass is calculated based on the volume of the submerged part (monopile) and the density of the respective surrounding material. In the case of soil, added mass is the sum of soil mass inside the pile and around the pile, where the tributary area to compute the soil mass inside  $(m_i)$  and around the monopile  $(m_s)$  is considered equivalent to the monopile area  $(m_i = m_s = A_p \rho_s)^{46}$ . It is also noted that this additional effective mass is considered for the horzontal component only. This is implemented by increasing the effective density of monopile in seawater (8880 kg/m<sup>3</sup>) and in soil (11,450 kg/m<sup>3</sup>) for all simplified models (M2-M5). In the full 3D model (M1), the soil domain is simulated by the continuum elements, where the gravitational forces are applied directly, which covers the inertial loading due to soil pile interaction. As modeling the water-pile interaction is not straightforward in the current Abaqus program, an alternative added mass method based on Equation 3 is considered in literatures. 17,46,48 The same method is also adopted this study for full 3D model to capture the approximate water-pile interaction effects.

$$m_{water} = C_a A_p \rho_w \tag{3}$$

$$m_{soil} = 2A_p \rho_s \tag{4}$$

where  $m_{water}$  and  $m_{soil}$  are the added masses per unit pile length for surrounding water and soil, respectively,  $C_a$  is the added mass coefficient, which is assumed to be 1.0, as suggested in (DNV<sup>55</sup>),  $A_p$  is the cross-section of the monopile,  $\rho_w = 1030 \text{ kg/m}^3$  is the seawater density, and  $\rho_s = 1800 \text{ kg/m}^3$  is the density of submerged soil.

FIGURE 4 Different foundation models: Full 3D (M1); Distributed spring (M2); Lump spring (M3); Improved apparent fixity (M4); Fixed at mudline (M5).

#### 3.2.1 | Foundation models

A *fixed-based model* is a very simple model to analyze the OWT. It supposes the surrounding soil has infinite stiffness; therefore, this model is also called the without SSI model (thereafter, w/o SSI model). This model is used to compare the importance of considering the soil-structure interaction in the dynamic response of the OWT. This can be achieved by fixing the pile at mudline level for all six degrees of freedom using the encastre boundary condition, as shown in Figure 4 (M5).

The *Improved apparent fixity model* is based on an extension of the fixity at an apparent depth below the mudline. In the traditional apparent fixity method, there is only one apparent beam used, whose apparent length (L) and bending rigidity (EI) are estimated by considering only the diagonal terms. However, in the improved apparent fixity model, two beams are added below the mudline consecutively to consider the off-diagonal terms in the traditional apparent fixity model, as shown in Figure 4 (M4).

$$F = [K]^{-1} = \begin{bmatrix} k_{hh} & k_{hr} \\ k_{rh} & k_{rr} \end{bmatrix}^{-1} = \begin{bmatrix} f_{uu} & f_{u\theta} \\ f_{\theta u} & f_{\theta \theta} \end{bmatrix}$$
 (5)

$$f_{uu} = \frac{1}{E_1 I_1} \left( \frac{L_1^3}{3} + L_1^2 L_2 + L_2^2 L_1 \right) + \frac{L_2^3}{3 E_2 I_2}$$
 (6)

$$f_{u\theta} = f_{\theta u} = \frac{1}{E_1 I_1} \left( \frac{L_1^2}{2} + L_1 L_2 \right) + \frac{L_2^2}{2E_2 I_2}$$
 (7)

**TABLE 4** Pile head stiffness used in this study for Apparent Fixity model.

Wind turbine	$k_{hh}$ (GN/m)	k <sub>rr</sub> (GN-m/rad)	$k_{hr}$ (GN-m/m)	L <sub>1</sub> (m)	L <sub>2</sub> (m)	$E_1$ (GN/m <sup>2</sup> )	$E_2$ (GN/ $m^2$ )
Lely A2	0.412	21.98	-2.35	5.00	11.09	105.34	354.62
Irene Vorrink	0.321	12.16	-1.21	5.00	9.86	108.97	402.69
Kentish Flats	0.953	45.93	-5.14	5.00	10.64	106.02	384.40
Walney 1	1.271	144.17	-10.54	5.00	17.21	91.01	287.15
North Hoyle	1.203	45.80	-5.76	5.00	9.47	109.96	449.31
NREL 5MW	1.698	130.94	-11.56	5.00	13.93	96.98	322.96

**TABLE 5** Formulation of monopile head stiffness for lump spring model.

	Soil profile		
Pile head stiffness	Constant	Linear	Parabolic
$K_{hh}$	$E_s d \Big(rac{E_p}{E_s^d}\Big)^{0.21}$	$0.6E_s d \Big(rac{E_p}{E_s^d}\Big)^{0.35}$	$0.8E_{_S}d\Big(rac{E_p}{E_s^d}\Big)^{0.28}$
$\mathbf{K}_{\mathbf{rr}}$	$0.15 E_s d^3 \left(\frac{E_p}{E_s^d}\right)^{0.75}$	$0.15E_s d^3 \Big(rac{E_p}{E_s^d}\Big)^{0.80}$	$0.15E_{s}d^{3}{\left(rac{E_{p}}{E_{s}^{d}} ight)}^{0.77}$
$\mathbf{K}_{\mathrm{hr}}$	$-0.22E_sd^2\Big(rac{E_p}{E_s^d}\Big)^{0.5}$	$-0.17E_{_{S}}d^{2}{\left(rac{E_{p}}{E_{s}^{d}} ight)}^{0.6}$	$-0.24 E_s d^2 \left(\frac{E_p}{E_s^d}\right)^{0.53}$
K <sub>z</sub>	$1.9E_sd\left(rac{L}{d} ight)^{rac{2}{3}}\left(rac{E_p}{E_s^d} ight)^{-\left(rac{L}{d} ight)}$	$1.8E_s d \left(rac{L}{d} ight)^{0.55} \left(rac{E_p}{E_s^d} ight)^{-rac{\left(rac{L}{d} ight)}{E_p^d}}$	$1.9E_sd\left(rac{L}{d} ight)^{0.6}\left(rac{E_p}{E_s^g} ight)^{-rac{\left(rac{J}{d} ight)}{E_g^d}}$

Note:  $E_s^d = E_{sDp}$  is the soil Young's modulus at a depth equal to the pile diameter  $D_p$ .  $L = L_e$  and  $d = D_p$ , are the monopile embedded length and outer diameter, respectively.  $E_n$  is the monopile Young's modulus.

$$f_{\theta\theta} = \frac{L_1}{E_1 I_1} + \frac{L_2}{E_2 I_2} \tag{8}$$

Although there is the possibility of a different combination of the parameters of two beams that could give the required flexibility terms, to make it simple, the second moment of inertia is kept the same as the monopile at the mudline  $(I_1 = I_2 = I)$ . Assuming the length  $L_1$  of the upper beam, only three unknown parameters (i.e.,  $L_2$ ,  $E_1$ , and  $E_2$ ) can be determined from the flexibility matrix [F] of the two-beam system given by Equations (5) to (8), where  $k_{\rm hh}$  is the horizontal stiffness,  $k_{\rm rr}$  is the rotational stiffness, and  $k_{\rm hr} = k_{\rm rh}$  are the coupled stiffness terms at the mudline level whose value is derived from load-displacement curves obtained from the 3D FEM simulation. A more detailed discussion can be found in literatures. 8,56,57 Table 4 shows the parameters computed by this procedure.

The *Lump Spring model* is based on the monopile head stiffness at the mudline level. There are several formulations to calculate the stiffness coefficient.  $^{31,58,59}$  However, all the formulations were verified based on a fundamental natural frequency only. As the primary aim of this study is to investigate higher mode effects, the monopile head stiffness is estimated using the expressions of Gazetas (1991),  $^{31}$  which have been commonly used in practice. For clarity, the expressions to calculate monopile head stiffnesses are tabulated in Table 5, where  $k_{\rm hh}$  is the horizontal stiffness,  $k_{\rm rr}$  is the rotational stiffness, and  $k_{hr} = k_{rh}$  are the coupled stiffness terms at the mudline. Their value can be determined by knowing the initial soil modulus of the seabed, pile modulus, and pile dimension which are the same used for Full 3D model. To create this foundation model, a cartesian plus rotation-type connected section is generated under the interaction module, which requires the value of the 6 × 6 symmetrical stiffness matrix [D].

The *Distributed spring model* is the most popular simplified model in literature due to its simplicity and efficiency. In this approach, a monopile is assumed to behave as Euler–Bernoulli beam of flexural rigidity ( $E_pI_p$ ), and soil is replaced by a set of independent springs distributed along the monopile embedded depth in both horizontal and vertical directions. The initial slope of non-linear curves (p-y, t-z, and q-z) is used to compute the linear modal analysis responses of an OWT. The p-y, t-z, and q-z curves used in practice are those recommended by American Petroleum Institute (API<sup>22</sup>) guidelines or Det Norske Veritas (DNV<sup>55</sup>) guidelines. It should be noted, however, that those curves were calibrated mainly against the response of small-diameter (610 mm) slender piles with a length-to-diameter ratio of 34 for the design of offshore oil and gas structures. The monopile used in modern OWTs is large in diameter (3–10 m), has a length-to-diameter ratio (3–6), and behaves as a rigid body, which is different from conventional bending pile.<sup>27</sup> Therefore, API-based p-y curves may not be suitable for large-diameter monopiles.<sup>17,22–24,60</sup>

The formulation of the non-linear soil springs, *p-y*, *t-z*, and *q-z* curves recommended in API guideline for cohesionless soil, which is used in this study and is briefly described in this section.

For sand below the water table, ultimate soil resistance per unit length of monopile depends on submerged unit weight  $\gamma'$  and internal friction angle  $\phi$ , expressed by Equation 9 as follows:

$$P_{u} = min \begin{cases} \gamma'Z \left[ \frac{K_{o}Ztan\phi sin\beta}{\tan{(\beta - \phi)}\cos{\alpha}} + \frac{tan\beta\left(D_{p} + Ztan\beta tan\alpha\right)}{\tan{(\beta - \phi)}} + K_{o}Ztan\beta\left(tan\phi sin\beta - tan\alpha\right) - K_{a}D_{p} \right] \\ \gamma'ZD_{p} \left[ K_{a}(\tan^{8}\beta - 1) + K_{o}tan\phi tan^{4}\beta \right] \end{cases}$$

$$(9)$$

where  $\alpha = \frac{\phi}{2}$ ,  $\beta = 45 + \frac{\phi}{2}$ ,  $K_o = 0.4$ ,  $K_a = \tan^2(45 - \frac{\phi}{2})$ ,  $\gamma'$  is average effective unit weight from ground surface to p-y curve, z is depth from the ground surface to p-y curve,  $D_p$  is outer diameter of monopile.

The *p-y* curves are generated according to Equation 10:

$$p = AP_{u} \tanh (kZy/AP_{u}) \tag{10}$$

where A is a factor to account for static or cyclic loading conditions. In this study, A = 0.9 is taken as recommended in API<sup>22</sup> for cyclic loading, k is the rate of increase of the initial modulus of subgrade reaction with depth and it depends on the internal friction angle ( $\phi$ ). The value of k is recommended in API design code<sup>22</sup> as a function of the friction angle of the sand.

The axial capacity of the monopile in the soil is modeled by a combination of shaft friction and end bearing capacity at the monopile tip, as described in the API guidelines. The t-z curve is used to represent the relationship between the mobilized soil-monopile shear transfer and displacement at any depth. Similarly, the q-z curve represents the relationship between the end bearing resistance and vertical deflection at monopile tip displacement. The API<sup>22</sup> recommends the values of  $t/t_{max}$  versus  $z/z_{peak}$  and  $q/q_p$  versus  $z/D_p$  in tabulated form for both sand and clay soils, which are not reported here for the brevity of the paper. Note that  $t_{max}$  is the maximum soil-monopile adhesion (unit shaft friction) and  $z_{peak}$  is the corresponding displacement. The recommended value of  $z_{peak}$  is 1% of the monopile diameter ( $D_p$ ). And q and  $q_p$  here are the mobilized and end bearing capacities corresponding to tip displacements of z and  $z_{peak}$ .

For implementation of this model, the embedded depth of the monopile is discretized along the length at some spacing (1 m is considered in this study) and is named a node. At each node, the nonlinear *p-y* spring (which represents the lateral resistances of the soil against the foundation movements) is applied in the horizontal direction, and the nonlinear *t-z* spring (which represents the shaft friction against the surrounding soil) is applied in the vertical direction. Finally, at the bottom of the monopile, a *q-z* spring (which depicts the end bearing capacity of the monopile) is applied, as shown in Figure 4 (M2). The implementation of non-linear springs can be repetitive and time-consuming in cases where a large number of springs are included in the finite element model; therefore, a Python code is developed to minimize the implementation time. Practically speaking, the initial stiffness of the nonlinear *p-y*, *t-z*, and *q-z* springs is sufficient for the linear modal analysis of the OWT. There is no need to include damping as well; however, one may use the same model for nonlinear analysis.

The full 3D model explicitly considers the 3D soil continuum. Complex foundation geometries, interface nonlinearities, and gap formulations with sophisticated constitutive laws can be modeled by this method. A 3D soil domain is created to account for the interaction between the monopile foundation and the surrounding soil. The size of the soil domain and boundary conditions significantly influence the dynamic behavior of an OWT.<sup>2</sup> The 3D modeling technique has been used by various investigators and researchers for rigorous modeling of the soil-monopile system. For instance, Alkhoury et al.<sup>17</sup> predicted fundamental natural frequency by restraining the soil domain in the horizontal direction and using weightless linear material as well as a large number of elements in the soil domain. This kind of consideration is not accurate for the prediction of higher-mode responses. In this study, some special treatment on boundary conditions is made, and full integration element type is used. The height of the soil domain is chosen at  $1.7L_e$  whereas the diameter is divided into two regions: the near-field region and the far-field region. The near-field region has a diameter of  $13D_P$ , whereas the far-field extends sufficiently so that an infinite soil boundary can be imposed, as shown in Figure 4 (M1). Note that  $D_P$  is the outer diameter and  $L_e$  is the embedded depth of the monopile in the soil domain. The infinite element boundary condition is applied in the lateral direction while the base of this domain is fixed in all directions. The advantages of using a combination of finite and infinite elements rather than just finite elements are that it reduces the size of the soil geometry,

and no external boundary conditions need to be specified. The soil, near-field region soil, and inside the monopile are modeled using linear three-dimensional 8-node brick elements with full integration (C3D8), whereas CIN3D8, a three-dimensional linear brick with 8 nodes, is used to model the infinite region (far-field). The contact between soil and pile is modeled using the surface-to-surface contact option. To implement the contact, normal and tangential behavior must be specified. For normal behavior, "hard" contact with the direct standard constraint enforcement method is used, whereas for tangential behavior, the penalty algorithm is chosen as the constraint enforcement method with a friction coefficient between the surfaces in contact of 0.5. Figure 4 (M1) shows the full 3D model of the wind turbine, including the soil domain and the corresponding mesh.

As the purpose of this study is to investigate the higher mode response based on linear modal analysis, which is concerned with very small amplitude vibration, the linear initial foundation stiffness soil model is sufficient to capture those effects.<sup>61</sup> It is also noted that simplified models (M2-M3) show a dashpot, which also does not affect the modal analysis response. The purpose of showing dashpot is to generalize the model for other analyses, like non-linear time history analysis. One of the purposes of this study is to compare the dynamic soil-structure response for three different soil profiles (constant, linear, and parabolic); however, there is no explicit option to vary the field variable with depth or time in Abaqus/CAE.<sup>44</sup> Therefore, a user's subroutine USDFLD code is implemented, which enables the simulation of models in which the properties of their materials are related to some parameters or conditions, such as the elastic modulus being related to its depth in this study. The soil properties used in this study are tabulated in Table 3.

#### 4 | HIGHER MODE AND MODAL ANALYSIS

Complex structures are typically examined under a wide range of dynamic operating circumstances to make sure the design will satisfy the specified functional requirements. A relatively limited number of these operational circumstances are chosen as critical during design optimization, and they are then used to either minimize or maximize the objective function. As the dynamic response is highly reliant on the structure's physical properties, monitoring them at the initial stage leads to large computational cost savings and optimizes the design. Modal analysis is a powerful technique to identify the inherent dynamic characteristics of OWTs, such as natural frequencies (eigenvalues), mode shapes (eigenvectors), effective mass participation, and damping characteristics.<sup>62</sup> Those characteristics are very important to calculate the dynamic response due to cyclic loads like earthquakes, wind, and waves. The modal analysis uses the overall mass and stiffness of a structure to find the various natural periods. The modal analysis is briefly described in this section. For more details, the reader may refer to Chopra (2007)<sup>62</sup> and Paz and Kim (2019).<sup>63</sup>

The general equation of motion for multi-degree of freedom (MDOF) is described by Equation 11:

$$[M] \{ \dot{U} \} + [C] \{ \dot{U} \} + [K] \{ U \} = F(t)$$
(11)

where [M], [C], and [K] are the mass, damping, and stiffness matrix, respectively. U is the displacement and is a function of space and time, that is, U = U(x,t).  $\dot{U}$  and  $\dot{U}$  are time derivatives of the displacement U, namely the velocity and acceleration of the system. The damping is generally ignored, and the force term is set to zero in vibrational modal analysis. By assuming free vibration as a simple harmonic and imposing its solution, the above differential Equation 12 can be written as:

$$\left[ \left[ K \right] - \omega_n^2 \left[ M \right] \right] \phi_n = 0 \tag{12}$$

Equation 12 is known as a "characteristic equation or frequency equation." The N roots for  $\omega_n^2$  are known as eigenvalues or characteristic values, and the eigenvectors or natural modes of vibration  $(\phi_n)$  corresponding to the natural frequencies of N modes of vibration can be obtained. In complex structures, there are thousands or millions of degrees of freedom and, as a result, millions of natural frequencies. However, each natural frequency is not equally important, so it is not necessary to extract the natural frequency of all the modes in finite element analysis. The way to judge the important higher modes is based on their mode participation factor  $(\Gamma_n)$  or the effective mass participation  $(M_{eff,n})$  of the nth mode, which can be calculated as follows:

$$\Gamma_n = \frac{\{\phi\}_n^T [M] \{D\}}{\phi_n^T [M] \phi_n}, \quad M_{eff,n} = \Gamma_n^2 \left(\phi_n^T [M] \phi_n\right)$$

$$\tag{13}$$

where {D} is the excitation direction vector (assumed as unit displacement vector) and it depends on the direction of excitation in each global cartesian direction and rotation about each of these axes.

The modal participation factor is a measure of how strongly a given mode contributes to the response of the structure when subjected to force or displacement excitation in a specific direction. The effective mass participation associated with each mode represents the amount of system mass participating in that mode in a given excitation direction. This value is given as a percentage of the total system mass. Therefore, a mode with a large effective mass will be a significant contributor to the system's response in the given excitation direction. A common rule of thumb for linear dynamic analysis is that a mode should be included if it contributes more than 1%–2% of the total effective mass, or cumulative effective mass should be at least 80%–90% of the total mass of the system in the predominant direction of excitation vibration. 62–65 It can be proven analytically (Clough and Penzien<sup>66</sup>) that the sum of the effective modal mass for all the modes of the structure is equal to the total mass of the structure, Equation 16, which is most convenient in assessing the number of significant modes of vibration to consider in the design.

$$\sum_{n=1}^{N} M_{eff,n} = \sum_{i=1}^{m} M_i \tag{14}$$

where m is total nodes in the structure

The effects of higher mode on offshore wind turbines can be visualized from the response spectrum of wind, wave, and earthquake, as shown in Figures 1A,B through response spectrum analysis (RSA). A response spectrum is a plot of the peak or steady-state response (displacement, velocity, or acceleration) of a series of single degree of freedom (SDOF) systems of varying natural frequency or period that are oscillated by the same base motion, shock, or earthquake. <sup>67</sup> As shown in Figure 1B, response-spectrum analysis is one of the linear-dynamic analysis methods that measure the contribution from each natural mode of vibration to indicate the likely maximum seismic response of structures. The maximum seismic response like displacement, base shear, and overturning moment is related to the modal participation factor of the nth mode natural frequency, and the peak response (displacement, velocity, and acceleration) corresponding to the same natural frequency from response spectra is given by Equations 15–17.

Displacement 
$$(u_n^i) = \Gamma_n^i \phi_n^i S_{d,n}$$
 (15)

Base shear 
$$(V_n) = \sum_{i=1}^m M_{eff,n}^i S_{a,n}^i$$
 (16)

Overturning moment 
$$(M_n) = \sum_{i=1}^{m} M_{eff,n}^i S_{a,n}^i h^i$$
 (17)

where  $S_{D,n}$  and  $S_{a,n}$  is, respectively, the spectral displacement and spectral acceleration for the nth mode. Its relationship can be represented as  $S_{a,n} = \omega_n^2 S_{d,n}$ .

# 5 | RESULTS AND DISCUSSIONS

This study has adopted five numerical models widely used in the literature for the analysis of the dynamic response of OWT (Kaynia, <sup>36</sup> Løken and Kaynia, <sup>8</sup> Alkhoury et al., <sup>17</sup> Yang et al., <sup>53</sup> Zuo et al. <sup>45</sup>). To ensure a robust correlation among the results given by different models, the determination of model parameters (standardization of models) is based on procedures widely accepted in engineering practice and uses the same mechanical material properties (input data) for each model. The input model parameters for the simplified foundation model are correlated with the mechanical properties of the material and are mentioned in various codes (API, <sup>22</sup> DNV<sup>23,55</sup>) and technical papers (Løken and Kaynia, <sup>8</sup> Gazatas, <sup>31</sup> Sunday and Brennan <sup>52</sup>). Although the simplified foundation models are widely accepted by researchers or practitioners for the calculation of the fundamental frequency of small-capacity wind turbines, their capability of predicting higher vibration modes for modern OWT with real geometric configurations is not clear. As the dynamic response is not only dependent on fundamental frequency but also on other inherent modal responses like higher modes, effective mass participation, and damping of the models as well, one of the aims of this paper is to investigate the capabilities of the simplified models for predicting higher mode effects compared with the full 3D model. The comparison of the different models is

TABLE 6 Calculated and measured fundamental natural frequencies (in Hz) for real offshore wind turbines using different foundation models.

		Wind farr	ns name			
Foundation models	Soil profile	Lely A2	Irene vorrink	Kentish flats	Walney 1	North hoyle
M1: Full 3D	Constant	0.639	0.543	0.327	0.344	0.363
	Linear	0.666	0.550	0.329	0.350	0.365
	Parabolic	0.664	0.549	0.337	0.348	0.364
M2: Distributed spring (API 2014)	Constant	0.612	0.554	0.321	0.331	0.351
	Linear	0.610	0.548	0.317	0.328	0.347
	Parabolic	0.608	0.550	0.318	0.318	0.348
M3: Lump spring (Gazatas 1991)	Constant	0.666	0.549	0.327	0.324	0.363
	Linear	0.684	0.562	0.334	0.360	0.371
	Parabolic	0.662	0.546	0.324	0.344	0.360
M4: Improved apparent fixity	Constant	0.638	0.522	0.313	0.327	0.347
(Løken and Kaynia 2019)	Linear	0.610	0.540	0.323	0.342	0.358
	Parabolic	0.631	0.515	0.308	0.320	0.358
M5: Fixed at mudline	_	0.736	0.599	0.358	0.401	0.399
Measured	-	0.634	0.546	0.339	0.350	0.350

made with reference to the same physical problem with common mechanical properties. Furthermore, compared with the 3D finite element models in the literature, we have also made several useful simplifications for the nacelle, rotor, and blade assembly, along with the use of a high-performance element type (20-noded brick element) and boundary conditions for better prediction of the higher mode effects. Therefore, the findings resulting from this study provide useful insights and practical implications that should be interesting to researchers and professionals.

# 5.1 | FEM model verification and validation

The most widely used method for solving mathematical models of engineering problems is the finite element method (FEM). In order to make engineering predictions with quantified confidence and evaluate the performance of a finite element model for assumptions, effectiveness, accuracy, and the potential of modeling OWT, verification and validation are the first steps. Validation in FEM enables checking the simulation results with real-world results, whereas verification evaluates whether finite element analysis (FEA) is conducted properly.<sup>68</sup> To validate and verify the OWT models, five existing OWTs have been selected from five different wind farm sites in Europe, as shown in Table 1. The reasons for the selection of these wind turbines are the availability of the data required for analysis and their measured fundamental natural frequency. Furthermore, five different foundation models are investigated for each OWT, as shown in Figure 4. The modal analysis responses for each case are summarized in Table 6. It can be seen that the computed and measured fundamental frequencies are in excellent agreement with the full 3D (M1) model. However, there is some discrepancy in the computation for other foundation modeling techniques (M2-M4), and there might be an unacceptable discrepancy for higher mode responses, which can be seen in further analysis (Sections 5.2 and 5.3). Therefore, the full 3D model (M1) can be used as a reference model for further analysis. Finally, this confirms that the modeling assumptions and accuracy of the finite element model developed for the estimation of the dynamic response of OWTs in this study are satisfactory.

# 5.2 | Modal analysis results

The main aim of modal (eigenvalue) analysis is to identify the higher-mode inherent dynamic characteristics of the NREL 5MW reference wind turbine by explicitly considering geometrical properties. This study also ascertains the capability and accuracy to produce the major modal analysis results (natural frequency, effective mass participation, and mode shape) from different dynamic soil structure interaction modeling techniques (M1 to M5), as explained earlier in Section 3.2.1.



**TABLE** 7 Comparison of the first five (a) natural frequencies and (b) effective mass participation ratio obtained from the full 3D model (M1) and one obtained from simplified foundation models (M2-M5).

		Natura	ıl frequ	ency (Hz)	(Deviation	n %)						
Mode	Mode shape	M1		M2		M3		M4		M5		
1	Tower bending (first order)	0.212	-	0.206	(-3.1)	0.217	(2.1)	0.209	(-1.3)	0.230	(8.3)	
2	Tower bending (second order)	1.278	-	1.203	(-5.9)	1.320	(3.2)	1.245	(-2.6)	1.445	(13)	
3	Tower bending (third order)	2.638	-	2.497	(-5.4)	2.733	(3.6)	2.568	(-2.7)	3.012	(14.1)	(a)
4	Tower bending (fourth order)	5.049	-	4.772	(-5.5)	5.283	(4.6)	4.908	(-2.8)	5.877	(16.4)	
5	Tower bending (fifth order)	9.095	-	8.619	(-5.2)	9.445	(3.9)	8.813	(-3.1)	10.56	(16.1)	
		Effecti	ve mas	s participa	ition ratio	(%) (Dev	riation %)					
Mode	Mode shape	M1		M2		M3		M4		M5		
1	Tower bending (first order)	37.23	-	38.4	(3.2)	40.6	(8.9)	44.3	(19.0)	51.9	(39.3)	
2	Tower bending (second order)	12.64	-	14.5	(14.3)	16.5	(30.7)	15.8	(25.3)	13.6	(7.9)	
3	Tower bending (third order)	7.67	_	7.6	(-1.3)	10.2	(32.9)	8.8	(15.2)	9.8	(27.3)	(b)
4	Tower bending (fourth order)	6.32	-	5.6	(-11.6)	7.5	(18.3)	6.9	(9.1)	7.8	(23.0)	
5	Tower bending (fifth order)	6.59	_	4.3	(-34.7)	4.2	(-35.9)	3.4	(-48.9)	4.2	(-35.5)	
	Sum:	70.4		70.3		79.0		79.2		87.3		

The first five-tower bending modes in the fore-aft direction (thereafter just called the first-five modes) are considered in this study because the tower and foundation have axially symmetric shapes and properties that give similar side-to-side direction results. The computed natural frequencies and the corresponding effective mass participation and mode shape are shown in Table 7 and Figure 6, respectively. It is noted that around 35 modes need to be extracted to achieve those first five modes. It can be seen that the natural frequencies obtained from different simplified foundation models (M2, M3, and M4) are quite similar compared to the full 3D model (M1), with a maximum deviation of 3.1%. However, there is a discrepancy in predicting first-mode effective mass participation from those simplified models compared to the full 3D model, with a maximum deviation of around 19%. It is also observed that none of the simplified foundation models (distributed spring, lump spring, and improved apparent fixity) agrees with the full 3D model for the estimation of higher mode responses (natural frequency and corresponding effective mass participation). The deviation in responses is increasing for higher modes, as shown in Figure 5. The deviation results for the higher mode responses in terms of natural frequency is around 3%–6%, whereas, in terms of effective mass participation, it is 14%–49%, as shown in Table 7. This may be due to, first, a lack of explicit consideration of higher mode responses to calibrate the simplified model, and second, the effects of pile deformability, especially rotation on the pile, leading to a coupling of the masses of the orthogonal directions.

It is also observed that the modal analysis results of the fixed-based model (M5) (without DSSI) and flexible-based models (M1–M4) (with DSSI) are significantly different. The natural frequencies of the M5 model are increased by 8%–16%, and effective mass participations are increased by around 8%–40% compared with the full 3D (M1) model. Therefore, non-consideration of DSSI effects and neglecting higher modes will lead to either an uneconomical or unsafe design.

Table 7 also shows that the summation of total mass participation in dynamic analysis for the reference model (Full 3D model) is only 70.4%, even after considering the first five bending modes, which is still less than the requirement as mentioned in various guidelines<sup>62–65</sup>; that means more higher modes need to be considered to make the dynamic response satisfactory. It is not appropriate to consider only the fundamental mode (effective mass participation is only around 37%) in dynamic analysis, especially in an earthquake-prone zone.

As the mode also plays an important role in the dynamic response of structures, the first five natural tower bending modes obtained from different foundation modeling techniques are compared, as shown in Figure 6, where all the modes

FIGURE 5 Comparison of modal response (natural frequency and effective mass participation) obtained from different foundation modeling techniques for higher modes of 5MW NREL wind turbine.

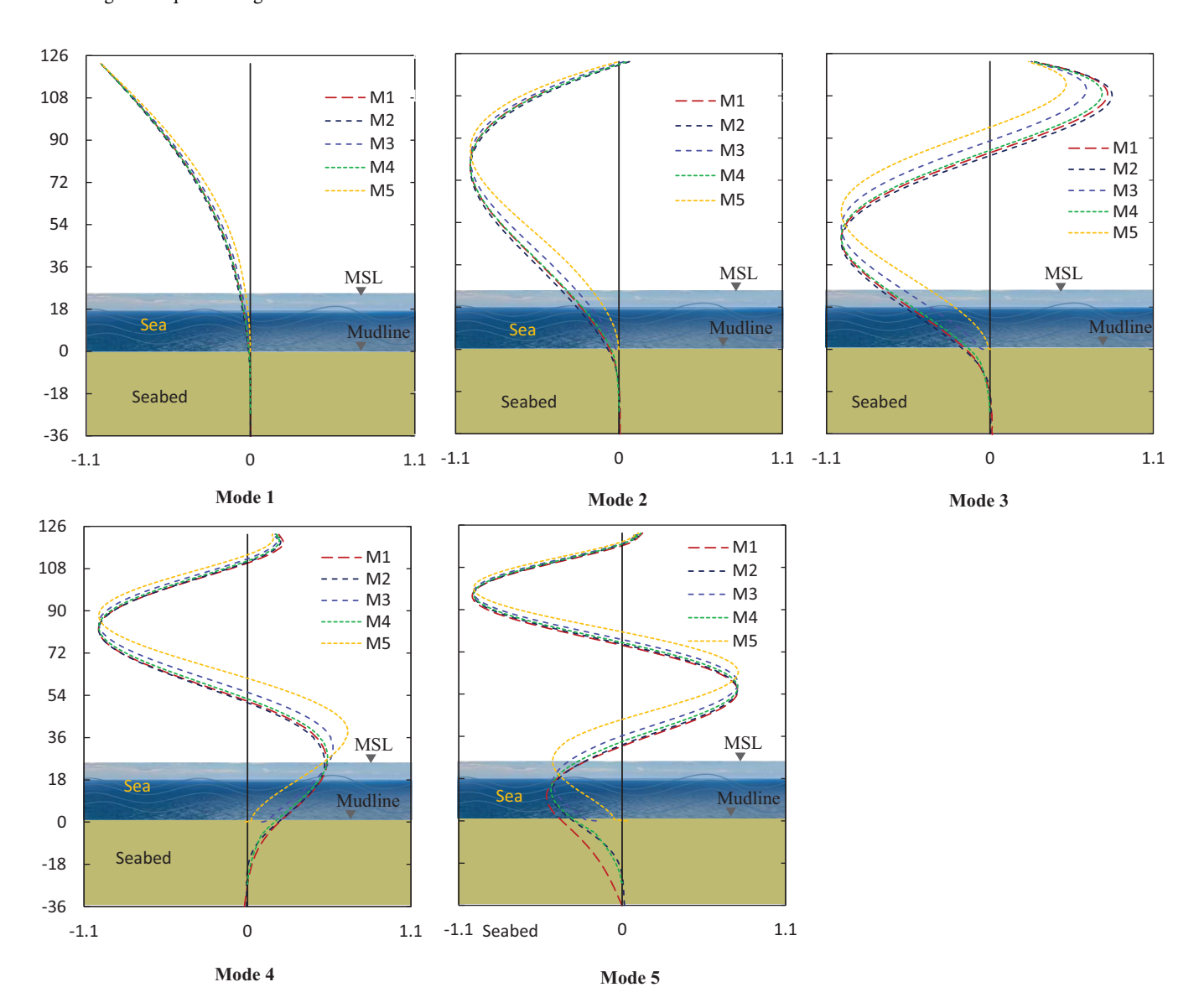


FIGURE 6 Comparison of first five mode normalized eigenvectors for different foundation models (M1-M5).

**TABLE 8** Deviation between spectrum analysis results estimated by considering fundamental mode only and the ones estimated by considering top five higher modes.

		Number of modes of	onsider	
Foundation models	Response	Fundamental: 1	Higher modes: 1-5	Difference (%)
M1: Full 3D	$\delta_{\rm t}  ({\rm mm})$	126.2	126.3	0.1
	$V_b(kN)$	368	989	169
	$M_o$ (kN-m)	2348	6055	158
M2: Distributed spring (API 2014)	$\delta_{\rm t}  ({\rm mm})$	134	135	0.7
	$V_b(kN)$	143	684	377
	$M_o$ (kN-m)	413	1087	163
M3: Lump spring (Gazatas 1991)	$\delta_{\rm t}  ({\rm mm})$	90.7	90.8	0.1
	$V_b(kN)$	254	1510	494
	$M_o$ (kN-m)	967	5020	419
M4: Improved apparent fixity (Løken	$\delta_{\rm t}  ({\rm mm})$	139	139	0.1
and Kaynia 2019)	$V_b(kN)$	402	978	143
	$M_o$ (kN-m)	1917	5656	195
M5: Fixed at mudline	$\delta_{\rm t}  ({ m mm})$	116.0	117.0	0.9
	$V_b(kN)$	742	1857	150
	$M_o$ (kN-m)	4155	10,014	141

*Note*:  $\delta_t$  = tower top displacement,  $V_b$  = base shear,  $M_o$  = overturning moment.

are normalized and the maximum displacement is set to unity. It is observed that the fundamental mode shapes are quite consistent with each other; however, they appear to disagree for higher modes. The deviation in mode shape along the height of the structure creates a challenge for optimizing the section of structures in design, which might lead to higher material costs.

Overall, the modal analysis results show that: (1) DSSI effects are significant; (2) higher modes need to be considered to get a reasonable dynamic response; and (3) none of the simplified DSSI models (M1–M4) can predict the dynamic response of higher modes satisfactorily.

# 5.3 | Response spectrum analysis results

Response spectrum analysis is a useful, inexpensive method for the preliminary design of a structure for a transient dynamic event such as earthquake base motion.<sup>67</sup> With the use of modal combination techniques, this method can be used to estimate the peak response (displacement, base shear, moment, etc.) by summing the contributions from each mode. As described in Section 4, the peak displacement (Equation 15), peak base shear (Equation 16), and peak overturning (Equation 17) of each mode mainly depend on the spectral response acceleration, effective mass participation, and mode shape of the corresponding mode. The spectral response acceleration is determined from either the design response spectrum or the site-specific response spectrum of a specific seismic zone. Figure 1B shows the ASCE 7 and EC8 design response spectra as well as some major earthquake site response spectra. In this study, the average site response spectrum is used to obtain the peak seismic demand of OWT. There are various methods for combining these peak responses in the individual modes to estimate the total peak response<sup>62</sup>; in this study, the square root of the sum of squares (SRSS) is adopted and given by Equation 18.

$$\left\{R\right\}_{max} = \sqrt{\sum_{n=1}^{n modes} \left|\left\{R\right\}_{max}^{n}\right|^{2}} \tag{18}$$

where n is the number of modes considered.

The comparison between the response obtained by considering only the fundamental mode and by considering higher modes (1–5) of the NREL 5 MW wind turbine is shown in Table 8. It is seen that higher modes have negligible effects on

**TABLE 9** First five natural frequencies and effective mass participation ratios for three different soil profiles estimated using the full 3D model (M1).

	Freque	Frequency [Hz] (Deviation %)							Eff. mass participation [%] (Deviation %)						
Mode	Consta	nt	Linear	Linear		lic	Constant		Linear		Parabo	lic			
1	0.211	-	0.212	(0.7)	0.211	(0.2)	37.2	-	37.2	(0.1)	37.1	(-0.1)			
2	1.272	-	1.278	(0.5)	1.277	(0.4)	12.8	-	12.6	(-1.4)	12.8	(-0.6)			
3	2.641	-	2.638	(-0.1)	2.650	(0.3)	6.8	-	7.7	(12.3)	6.5	(-4.8)			
4	5.062	-	5.049	(-0.3)	5.088	(0.5)	6.3	-	6.3	(0.9)	6.0	(-4.6)			
5	9.102	-	9.095	(-0.1)	9.182	(0.9)	6.5	-	6.6	(0.7)	5.1	(-21.3)			
						Sum:	71.5		70.4		65.4				

tower top displacement, whereas base shear and overturning moment have been significantly affected, with a maximum amplification of 169% and 158%, respectively. This result makes sense for three major reasons. First, fundamental natural frequency  $(f_1)$  falls in the zone below the peak spectral response acceleration, whereas higher mode natural frequency  $(f_2-f_5)$  falls in the peak spectral response acceleration zone, as shown in Figure 1B. Second, effective mass participation in the fundamental mode is around 37% of total effective mass only, whereas the rest of the mass ( $\sim$ 33%) belongs to higher modes, as shown in Table 7(b). Third, the OWT structure is quite different from tall conventional structures like tall buildings; in the case of OWT, heavy mass is located on the top of the turbine, whereas in tall buildings, mass is distributed almost uniformly along the height. By combining the effects of peak acceleration, effective mass participation, and moment lever arm, the above-obtained response can be visualized. Furthermore, the negligible effect on tower top displacement is because the frequency range  $(f_1-f_5)$  of OWT falls in the flatter zone of the displacement response spectrum, which is not shown here for brevity.

It is also observed that in the fixed-based model (M5), base shear and overturning moments are higher than in flexible-based models (M1-M4). This analysis result indicates that neglecting DSSI effects (comparing the fixed-based model (M5) with the flexible based (M1-M4)) overestimates the base shear and overturning moment, which leads to uneconomical design. On the other hand, neglecting higher modes (considering only the fundamental mode) underestimates the base shear and overturning moment and leads to unsafe design of OWT, especially in the seismic-prone zone.

# 5.4 | Parametric study

To get further insights into the dynamic behaviors of modern wind turbines, a parametric study is performed by varying some important design parameters. The results are produced for five different foundation models (M1-M5) to quantify the influence of soil inhomogeneity, initial soil modulus, and the monopile dimensions (embedded depth, diameter, and thickness) in terms of first five tower bending mode frequencies and corresponding effective mass participation in the fore-aft direction. In all cases, the same NREL 5MW superstructure properties as shown in Table 1 are used. The results are tabulated for the full 3D model (M1) only, whereas a comparison of results is made with all five foundation models (M1-M5) graphically to make the paper concise.

# 5.4.1 | Effect of soil inhomogeneity

Three different soil profiles are studied, namely constant (homogeneous), linear (non-homogeneous), and parabolic (non-homogeneous), as shown in Figure 2. For the selected soil profiles, soil domain size and pile dimension are assumed to be the same as shown in Table 5. For all three cases,  $E_{sD_p}=100~\rm kPa$  at  $z=D_p$  is considered for this analysis. Table 9 gives the first five natural frequencies and their corresponding effective mass participation, which are also plotted in Figures 7A,B. It is observed that the natural frequencies of the system change marginally with a maximum deviation of 0.9% for the three soil profiles, whereas the corresponding effective mass participation deviates significantly up to 21.3% for higher modes. It can also be noticed that the effect of soil inhomogeneity is more or less the same for all other simplified DSSI models (M2-M4). However, a linear soil profile is adopted for all other analyses.

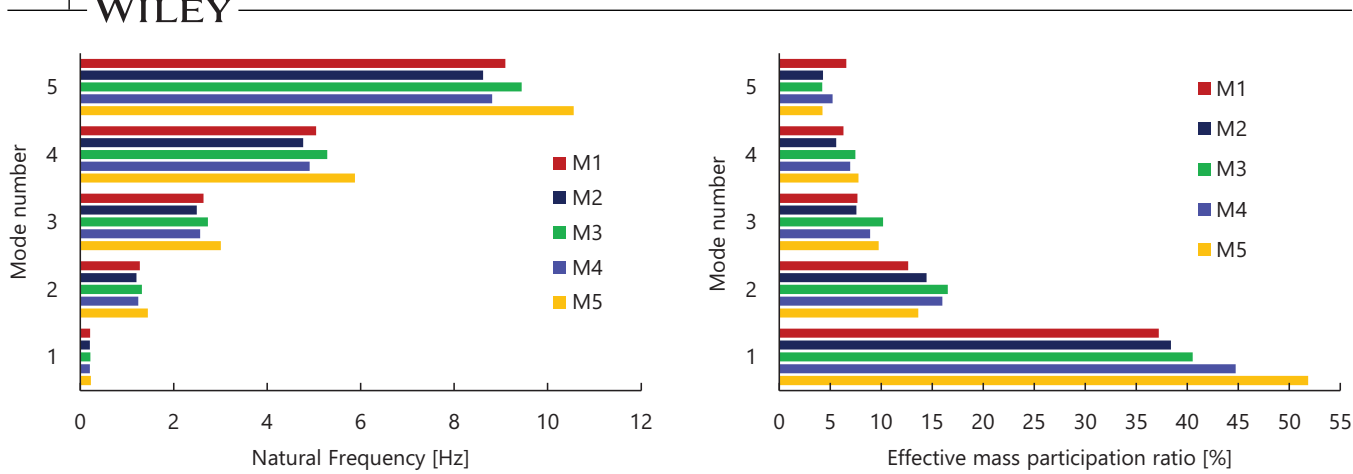


FIGURE 7 Comparison of soil inhomogeneity effects on (A) natural frequency and (B) effective mass participation ratio for top five modes obtained from different foundation models (M1-M5) for linear soil profile.

**TABLE 10** First five natural frequencies and effective mass participation ratios for three different initial soil moduli estimated using the full 3D model(M1).

	Freque	Frequency [Hz] (Deviation %)							Eff. mass participation [%] (Deviation %)						
Mode	Es = 50	Мра	Es = 100 MPa		Es = 15	0 MPa	Es = 50	0 MPa	Es = 100 MPa		Es = 150 MPa				
1	0.211	-	0.212	(0.7)	0.216	(2.4)	37.7	-	37.2	(-1.2)	36.9	(-2.1)			
2	1.255	-	1.278	(1.9)	1.306	(4.1)	13.5	-	12.6	(-6.7)	12.1	(-10.5)			
3	2.582	-	2.638	(2.2)	2.697	(4.5)	7.6	-	7.7	(0.3)	6.8	(-10.4)			
4	4.928	-	5.049	(2.5)	5.181	(5.1)	6.4	-	6.3	(-1.5)	5.6	(-12.6)			
5	8.849	-	9.095	(2.8)	9.410	(6.3)	6.2	-	6.6	(6.2)	3.9	(-36.5)			
						Sum:	71.5		70.4		65.4				

## 5.4.2 | Effect of soil initial modulus

Offshore monopile foundations are often found in sand of various initial modulus characteristics. To examine the effects of soil initial modulus, three different initial Young's moduli ( $E_{sDp}$ ) of 50, 100, and 150 MPa for loose, medium, and dense sand, respectively, are chosen in this study. The natural frequencies and corresponding effective mass participation are examined and compared between four different foundation modeling techniques (M1-M5). The results are tabulated in Table 10 for the full 3D model (M1) and comparison results between other DSSI models (M2-M4), as shown in Figure 8. It is seen that the natural frequencies of the system increase with the increasing value of soil initial stiffness (from loose to dense sand), whereas effective mass participation decreases with the increasing value of soil initial stiffness. Furthermore, the rise in the soil initial modulus (change from 50 to 150 MPa) increases the first natural frequency by 2.4% and decreases the corresponding effective mass participation by around 2.1%; however, this augmentation for the higher mode is equal to 6.3% and 36.1%, respectively. It can be observed that the results of the simplified DSSI models (M2-M4) do not match those of the full 3D model (M1).

# 5.4.3 | Effect of embedded monopile length

The monopiles behave rigidly or flexibly depending on pile bending stiffness compared to the surrounding soil stiffness and strength. Rigid (short) piles tend to rotate and translate like rigid bodies, whereas flexible (slender) piles tend to bend, as shown in Figure 2. The load capacity of a rigid pile is primarily governed by soil properties, whereas the load capacity of a slender pile is governed by the structural capacity of the pile. The pile length at which its ultimate capacity does not increase infinitely with depth is called the active length of the pile or critical embedded depth. <sup>69,70</sup> Therefore, the determination of the embedded length of the offshore monopile is an important parameter to optimize the cost of the foundation of an OWT system. In this section, the effect of monopile foundation depth is studied for medium-dense sand

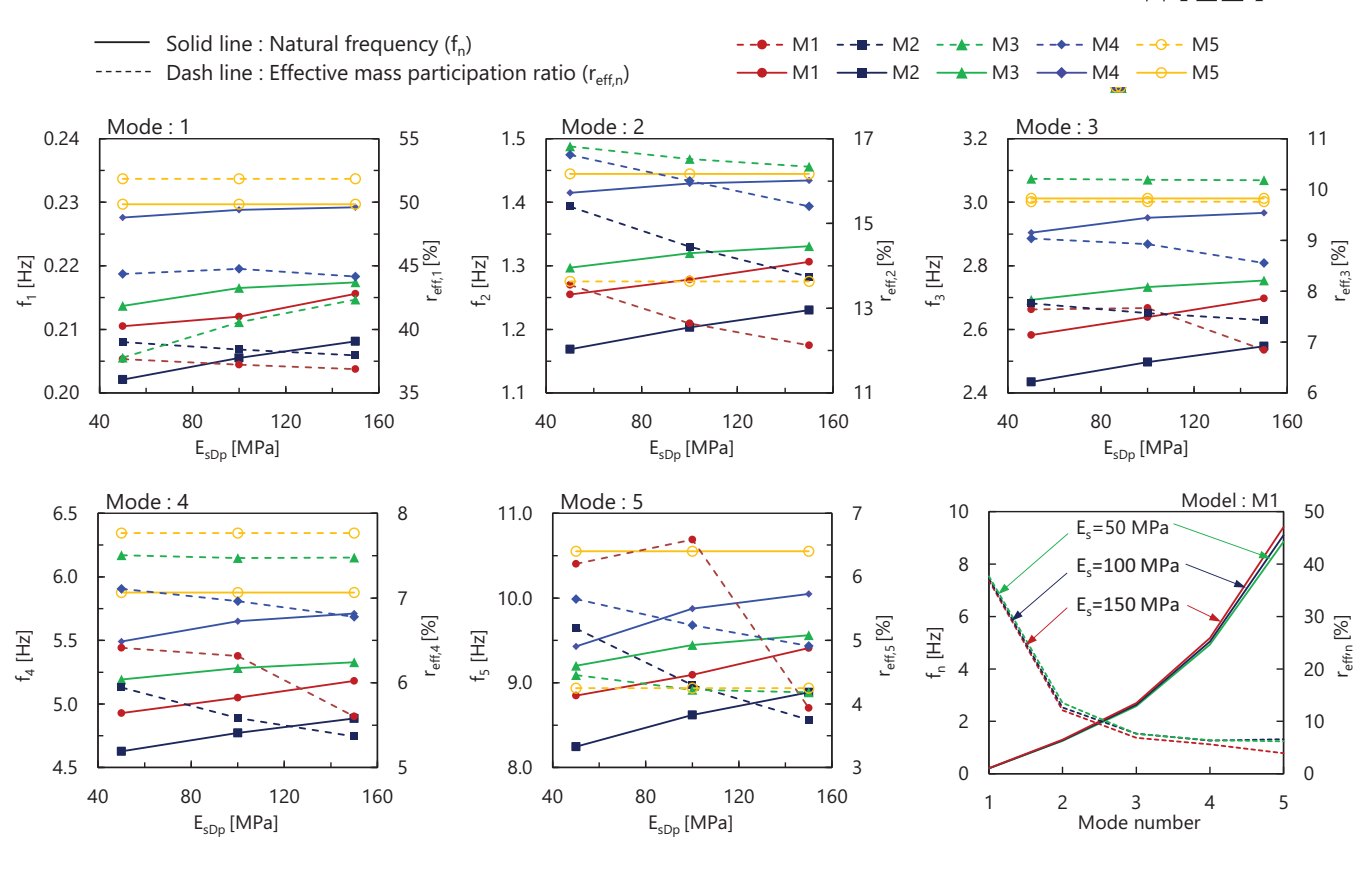
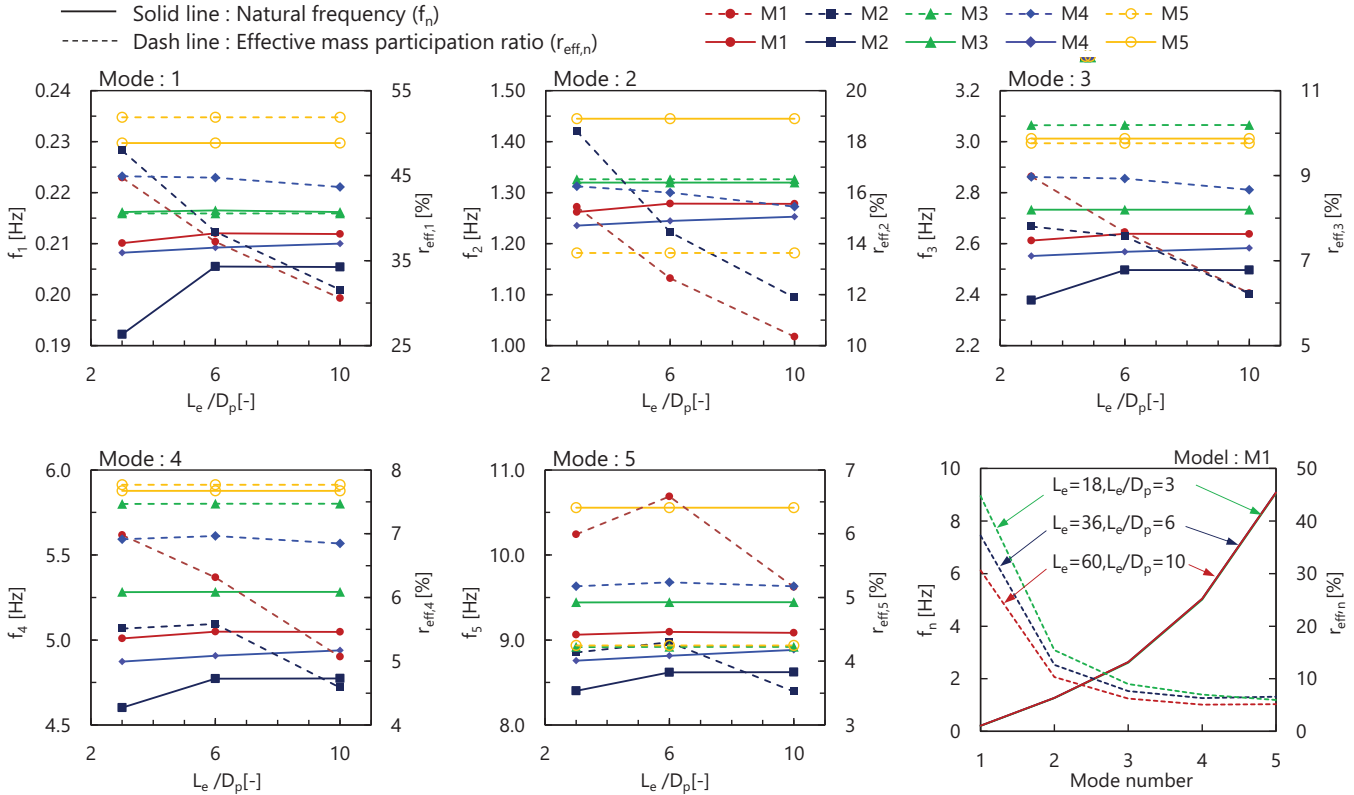


FIGURE 8 Comparison of the effect of initial stiffness on natural frequency and effective mass participation ratio obtained from different foundation models (M1-M5) for the top five modes.

**TABLE 11** First five natural frequencies and effective mass participation ratios for three different monopile embedded depth estimated using the full 3D model (M1).

	Freque	ncy [Hz	] (Deviatio	on %)			Eff. mass participation [%] (Deviation %)					
Mode	$L_e = 18$	m	$L_{e} = 36$	$L_e = 36 \text{ m}$		m	$L_e = 18 \text{ m}$		$L_e = 36 \text{ m}$		$L_e = 60$	) m
1	0.210		0.212	(0.9)	0.212	(0.9)	44.7	-	37.2	(-16.8)	30.6	(-31.6)
2	1.262	-	1.278	(1.3)	1.278	(1.3)	15.4	-	12.6	(-18.2)	10.3	(-33)
3	2.612	-	2.638	(1)	2.638	(1)	9.0	-	7.7	(-14.6)	6.2	(-30.6)
4	5.009	-	5.049	(0.8)	5.047	(0.8)	7.0	-	6.3	(-9.5)	5.1	(-27.3)
5	9.062	-	9.095	(0.4)	9.084	(0.2)	6.0	-	6.6	(9.9)	5.2	(-13.8)
						Sum:	71.5		70.4		65.4	

 $(E_{sDp}=100~{
m MPa})$  for three different values of embedded length  $(L_{
m e}=18,36,$  and 60 m). Note that the superstructure, soil domain size, monopile diameter  $(D_p=6~{
m m})$ , and monopile thickness  $(t_p=60~{
m mm})$  are chosen the same for all three cases as shown in Table 1. The selected monopile embedded length and diameter give  $L_{
m e}/D_{
m p}$  ratios of 3, 6, and 10, which covers a common range of values found in modern OWT foundation designs. The effects of monopile embedded length on modal response are presented in Figure 9 and Table 11. It is observed that at the start, natural frequency increases with an increase in the monopile embedded length, and then it becomes constant beyond the  $L_{
m e}/D_{
m p}$  ratio of 6, the so-called critical embedded depth. This is in agreement with the observation of Alkhoury et al. However, effective mass participation decreases with increasing embedded pile length. It is also seen that with the increase in the monopile embedded length from 18 to 60 m the value of natural frequencies increases marginally by about 1%, whereas a significant reduction in effective mass participation is about 33% for higher modes. This finding related to critical embedded depth is very useful for the optimization of the monopile design. Figure 9 compares the effect of embedded length obtained from different foundation modeling techniques (M1-M5) for the top five tower bending modes separately. Although the natural frequencies obtained



Comparison of the embedded depth effects on natural frequency and effective mass participation ratio obtained from different foundation models (M1-M5) for top five modes.

First five natural frequencies and effective mass participation ratios for three different monopile diameter estimated using the full 3D model (M1).

	Freque	Frequency [Hz] (Deviation %)							Eff. mass participation [%] (Deviation %)					
Mode	$D_p = 31$	$\overline{D_p = 3 m}$ $\overline{D_p = }$		$D_p = 12 r$		m	$D_p = 3$	$D_p = 3 m$		$D_p = 6 m$		2 m		
1	0.140	-	0.212	(51.1)	0.261	(86)	50.7	-	37.2	(-26.6)	21.7	(-57.2)		
2	1.060	-	1.278	(20.6)	1.656	(56.3)	11.6	-	12.6	(9.2)	7.5	(-34.9)		
3	2.460	-	2.638	(7.2)	3.259	(32.5)	5.4	-	7.7	(42.4)	16.7	(210.7)		
4	4.571	-	5.049	(10.5)	5.321	(16.4)	4.1	-	6.3	(53)	13.0	(214.9)		
5	8.330	-	9.095	(9.2)	9.953	(19.5)	1.9	-	6.6	(243.3)	8.3	(335.1)		
						Sum:	71.5		70.4		65.4			

from different simplified DSSI models (M2-M4) are somehow consistent with the full 3D model (M1), the effective mass participation ratio results are significantly different for all modes.

#### 5.4.4 Effect of monopile diameter and thickness

To design the foundation of modern offshore wind turbines, the diameter of the monopile plays a very important role in making the OWT system stable. Therefore, three different monopile outer diameters ( $D_p$ ), namely 3.6, 6, and 12 m, corresponding to  $L_e/D_p$  ratios of 10, 6, and 3, are investigated. In all three cases, monopile thickness ( $t_p = 60 \text{ mm}$ ) and embedded pile depth ( $L_{\rm e} = 36$  m) remain constant. The results are shown in Figure 10 and Table 12. It is observed that there is a significant increase in the frequency of about 86% with increasing pile outer diameter (from  $D_p = 3.6$  m to  $D_p = 12$  m), whereas the effective mass participation tends to decrease with increasing pile outer diameter by about 57%. These effects are more prominent in higher modes. This kind of effect is primarily due to an increase in foundation

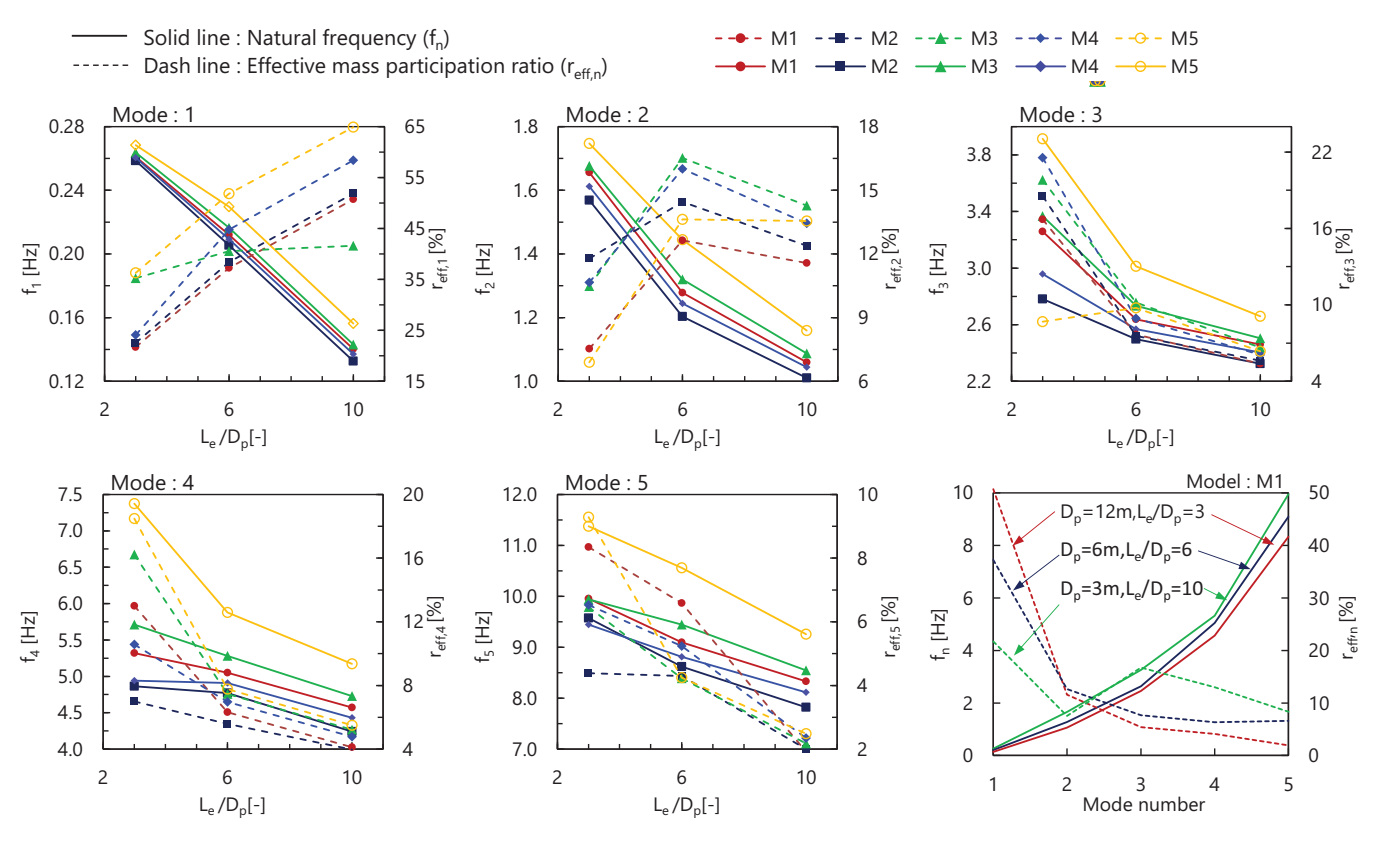


FIGURE 10 Comparison of monopile diameter effects on natural frequency and effective mass participation ratio obtained from different foundation models (M1-M5) for top five modes.

**TABLE 13** First five natural frequencies and effective mass participation ratios for three different monopile wall thickness estimated using the full 3D model (M1).

	Frequency [Hz] (Deviation %)						Eff. m	Eff. mass participation [%] (Deviation %)					
Mode	$T_p = 60 \text{ mm}$		$T_p = 75 \text{ mm}$		T <sub>p</sub> = 100 mm		$T_p = 60 \text{ mm}$		$T_p = 75 \text{ mm}$		T <sub>p</sub> = 100 mm		
1	0.212		0.221	(4.4)	0.231	(9.2)	37.2	_	32.5	(-12.6)	26.9	(-27.6)	
2	1.278	-	1.315	(2.9)	1.356	(6)	12.6	-	13.1	(3.9)	13.3	(5.02)	
3	2.638	-	2.647	(0.3)	2.616	(-0.8)	7.7	_	8.6	(11.9)	10.3	(33.9)	
4	5.049	-	5.031	(-0.4)	4.923	(-2.5)	6.3	-	6.7	(5.7)	6.3	(-0.2)	
5	9.095	-	9.187	(1.01)	9.123	(0.3)	6.6	_	7.7	(17.6)	5.7	(-13.7)	
						Sum:	71.5		70.4		65.4		

stiffness, especially the bending stiffness of the pile. Moreover, excessive reduction of monopile diameter with respect to monopile wall thickness and tower diameter may lead to local buckling and premature failure, as shown in Figure 10 for case  $L_{\rm e}/D_{\rm p}$  ratio 10. Its effects are prominent for the fixed-based model (M5) because stiffness differences become high at short distances (the length of the pile above the mudline is small). Therefore, care should be taken while designing the monopile. Figure 10 compares the effects of monopile diameter observed from different foundation modeling techniques. It can also be seen that there is an increase in frequency with increasing pile diameter and a decrease in effective mass participation with increasing pile diameter. However, the modal responses are significantly different for different foundation models, especially for higher modes.

Furthermore, the effects of monopile wall thickness are also investigated on modal response for three different thicknesses: 60, 75, and 100 mm. The monopile outer diameter ( $D_p = 6$  m) is considered for all three cases, and correspondingly, the ratios of pile diameter ( $D_p$ ) to wall thickness ratio ( $D_p/t_p$ ) are 100, 80, and 60, respectively. From Table 13 and Figure 11, one may observe that the natural frequencies of the OWT increase with the increase in monopile wall thickness. For instance, the first natural frequency increases by around 9.2% as the monopile wall thickness increases from 60 to 100 mm, whereas the corresponding effective mass participation decreases by around 27.6%. It is also seen that there is an increase

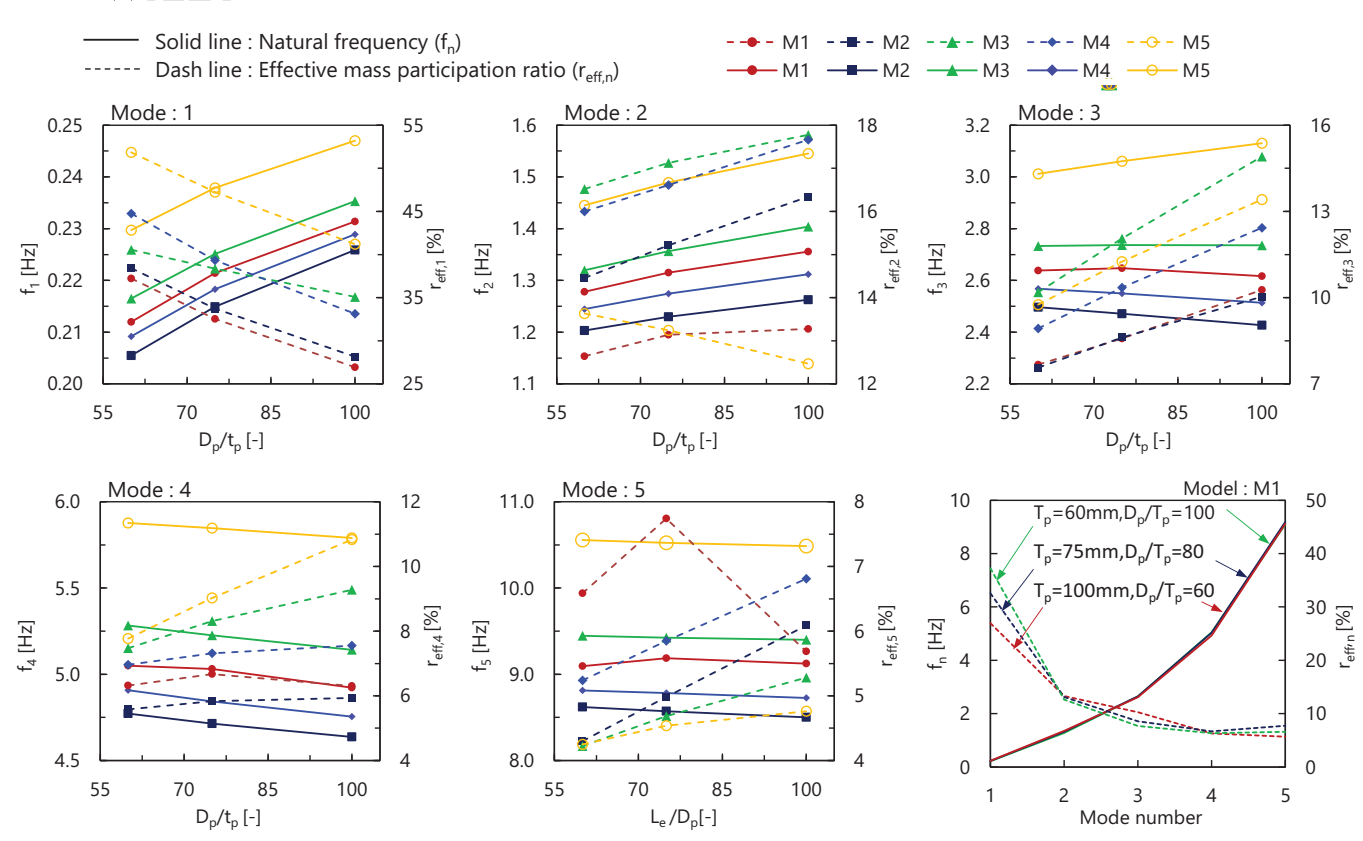


FIGURE 11 Comparison of monopile wall thickness effects on natural frequency and effective mass participation ratio obtained from different foundation models (M1-M5) for top five modes.

in fundamental frequency with the increase in monopile wall thickness for all simplified DSSI models; however, these effects are varied for higher modes. In terms of the effective mass participation ratio, a similar but the opposite trend is observed: there is a decrease instead of an increase in value.

# 6 | CONCLUSIONS

This study is aimed to investigate the effects of higher modes on the dynamic response of monopile-supported offshore wind turbines using the 3D finite element modeling technique and considering five simplified foundation models commonly used in practice. First, the modeling technique and assumptions are verified using natural frequency measurements for five real wind turbines at different European wind farms. Then, a detailed modal analysis using the verified modeling technique is carried out for the NREL 5 MW reference wind turbine, along with a detailed parametric study to examine the effects of higher modes. The following major conclusions can be drawn from this study:

- 1. The assumptions and geometric considerations chosen for modeling the OWT structure play an important role in obtaining the higher-mode dynamic response and have consequences in terms of computational cost. Different dynamic soil-structure interaction (DSSI) modeling techniques (M1-M5) may lead to different modal responses, especially for higher modes. Care should thus be taken in the selection of modeling techniques and the use of the results.
- 2. The modal analysis results yielded from the different simplified foundation models (distributed spring, lump spring, and improved apparent fixity) compared with those of the full 3D model are quite consistent in terms of higher-mode natural frequencies, with a maximal deviation of about 6%. However, in terms of effective mass participation, the deviation can be as large as 49%. Simplified models need to be improved to get a reasonable higher-mode response.
- 3. The consideration of DSSI effects significantly influences the modal response of the OWT system. Compared with the fixed base model, the natural frequency decreases by 8%–16% and the effective mass participation ratio increases by 8%–40% for the first five modes when using the flexible foundation models.

- 4. In terms of response spectrum, non-consideration of DSSI effects overestimates the base shear and overturning moment, thus leading to uneconomical design, whereas neglecting higher modes (considering only the fundamental mode) may underestimate the base shear and overturning moment, leading to unsafe design.
- 5. Higher-mode effects may amplify the seismic demand (base shear and overturning moment) by approximately 160%, whereas the effects on the tower top displacement of OWT may be negligible.
- 6. The contribution of higher modes depends mainly on the types of structure, nature of loading, and relative stiffness of the foundation and surrounding soil.
- 7. The effect of soil inhomogeneity (soil profile) on the modal response is minor. For all modes, the linear soil profile gives a slightly higher natural frequency compared to the constant and parabolic soil profiles.
- 8. The initial soil modulus affects the higher-mode modal response. The natural frequency of the system tends to increase, whereas the effective mass participation ratio decreases significantly if the initial soil modulus increases.
- 9. For all modes, an increase in the monopile embedded depth increases the natural frequency up to the critical embedded depth, after which its effect becomes negligible. However, effective mass participation decreases with increased embedded pile length. This critical embedded depth is thus a useful factor for optimizing the design of monopiles.
- 10. An increase in the monopile outer diameter and wall thickness significantly increases the natural frequency and decreases the effective mass participation of the OWT system. This is primarily due to an increase in foundation stiffness, especially the bending stiffness of the pile. Moreover, care should be taken that excessive reduction of monopile diameter with respect to wall thickness and tower diameter may lead to local buckling and premature failure.
- 11. Modal responses tend to deviate more and more towards higher modes for all simplified DSSI foundation models (distributed spring, lump spring, and improved apparent fixity). This is because most of these models are calibrated for fundamental mode only. Improvement is required when these models are used for the design of OWTs in the seismic vulnerability zone, for which higher modes can be important.

Last but not least, it is worth emphasizing that this study is based on numerical results obtained through modal analysis and linear response spectrum analysis, with particular attention to the role of higher modes in the seismic design of OWTs. To develop a more comprehensive understanding of the dynamic response of the OWT system, more advanced methods that incorporate non-linear time-history (dynamic) analysis, various damping mechanisms, kinematic soil-pile interaction, and sophisticated soil models are needed. However, the difficulty and uncertainty associated with the determination of model parameters and the computational cost involved should not be overlooked.

#### ACKNOWLEDGMENTS

The financial support provided by the Research Grants Council of Hong Kong (C7038-20G) is gratefully acknowledged.

### DATA AVAILABILITY STATEMENT

The data that support the findings of this study are available from the corresponding author upon reasonable request.

#### ORCID

Jun Yang https://orcid.org/0000-0002-0250-5809

#### REFERENCES

- 1. GWEC. Global Wind Energy Council. Global Wind Report, Annual Market Update; 2023.
- 2. Ma H, Chang X, Deng Y, Yang J. A simplified method for estimating the permanent accumulated rotation of an offshore wind turbine monopile throughout its design life. *Ocean Eng.* 2022;265(July):112664.
- $3. \ \ Ma\ H,\ Yang\ J.\ A\ novel\ hybrid\ monopile\ foundation\ for\ offshore\ wind\ turbines.\ \emph{Ocean\ Eng.}\ 2020;198:106963.$
- 4. Bhattacharya S, Biswal S, Aleem M, et al. Seismic design of offshore wind turbines: good, bad and unknowns. Energies. 2021;14(12):3496.
- 5. Mo R, Kang H, Li M, Zhao X. Seismic fragility analysis of monopile offshore wind turbines under different operational conditions. *Energies*. 2017;10(7):1037.
- 6. Kaynia AM. Seismic considerations in design of offshore wind turbines. Soil Dyn Earthq Eng. 2019;124:399-407.
- 7. Akay B, Ragni D, Ferreira CS, Van Bussel GJW. Investigation of the root flow in a Horizontal Axis. Wind Energy. 2013;17(7):1093-1109.
- 8. Løken IB, Kaynia AM. Effect of foundation type and modelling on dynamic response and fatigue of offshore wind turbines. *Wind Energy*. 2019;22(12):1667-1683.
- 9. Yang J, Li J, Lin G. A simple approach to integration of acceleration data for dynamic soil-structure interaction analysis. *Soil Dyn Earthq Eng.* 2006;26(8):725-734.

- 10. Álamo GM, Aznárez JJ, Padrón LA, Martínez-Castro AE, Gallego R, Maeso O. Dynamic soil-structure interaction in offshore wind turbines on monopiles in layered seabed based on real data. *Ocean Eng.* 2018;156(2016):14-24.
- 11. Christopoulos C, Zhong C. Towards understanding, estimating and mitigating higher-mode effects for more resilient tall buildings. *Resilient Cities Struct*. 2022;1(1):53-64.
- 12. Nair D, Ichihashi K, Terazawa Y, Sitler B, Takeuchi T. Higher mode effects of multistorey substructures on the seismic response of double-layered steel gridshell domes. *Eng Struct*. 2021;243(January):112677.
- 13. Maniatakis CA, Psycharis IN, Spyrakos CC. Effect of higher modes on the seismic response and design of moment-resisting RC frame structures. *Eng Struct*. 2013;56:417-430.
- 14. Wiebe L, Christopoulos C, Tremblay R, Leclerc M. Mechanisms to limit higher mode effects in a controlled rocking steel frame. 1: Concept, modelling, and low-amplitude shake table testing. *Earthq Eng Struct Dyn.* 2013;42(7):1053-1068.
- 15. Pennucci D, Sullivan TJ, Calvi GM. Prediction of Higher-Mode Response of Tall RC Wall Buildings. 15th World Conf on Earthq Eng (WCEE), Lisbon, Portugal, Sep, 2012.
- 16. De Risi R, Bhattacharya S, Goda K. Seismic performance assessment of monopile-supported offshore wind turbines using unscaled natural earthquake records. *Soil Dyn Earthq Eng.* 2018;109:154-172.
- 17. Alkhoury P, Soubra AH, Rey V, Aït-Ahmed M. A full three-dimensional model for the estimation of the natural frequencies of an offshore wind turbine in sand. *Wind Energy*. 2021;24(7):699-719. doi:10.1002/we.2598
- 18. Gupta BK, Basu D. Offshore wind turbine monopile foundations: design perspectives. Ocean Eng. 2020;213:107514.
- Ahmed SS, Hawlader B, Roy K. Finite element modeling of large diameter monopiles in dense sand for Offshore Wind Turbine Foundations. Proceedings of the ASME 34<sup>th</sup> International Conference on Ocean, Offshore and Arctic Engineering, St. John's, Newfoundland, Canada, May, 2015.
- 20. Lombardi D, Bhattacharya S, Muir Wood D. Dynamic soil-structure interaction of monopile supported wind turbines in cohesive soil. *Soil Dyn Earthq Eng.* 2013;49:165-180.
- Andersen LV, Vahdatirad MJ, Sichani MT, Sørensen JD. Natural frequencies of wind turbines on monopile foundations in clayey soils-A
  probabilistic approach. Comput Geotech. 2012;43:1-11.
- 22. API. Petroleum and Natural Gas Industries- Specific Requirements for Offshore Structures. Part 4 Geotechnical and Foundation Design Considerations. *American Petroleum Institute (API) Reccomended Practice*. 2011.
- 23. DNV. Support structures for wind turbines: DNVGL-ST-0126, Oslo, Norw DNV GL. 2016:182.
- 24. Byrne BW, Houlsby GT, Burd HJ, et al. PISA design model for monopiles for offshore wind turbines: application to a stiff glacial clay till. *Geotechnique*. 2020;70(11):1030-1047.
- 25. Wang Z, Hu R, Leng H, Liu H, Bai Y, Lu W. Deformation analysis of large diameter monopiles of offshore wind turbines under scour. *Appl Sci.* 2020;10(21):1-18.
- 26. Zdravković L, Taborda DMG, Potts DM, et al. Numerical modelling of large diameter piles under lateral loading for offshore wind applications. Front Offshore Geotech III—Proc 3rd Int Symp Front Offshore Geotech ISFOG 2015; 2015:759-764.
- 27. Ma Y, Yang J. Earth pressure distribution on laterally loaded offshore monopiles. Ocean Eng. 2023;273:113954.
- 28. Kausel E. Early history of soil-structure interaction. Soil Dyn Earthq Eng. 2010;30(9):822-832.
- 29. NIST. NIST GCR 12-917-21 soil-structure soil-structure interaction for building structures. Soil-Structure Interact Build Struct. 2012;12:292.
- Arany L, Bhattacharya S, Hogan SJ, Macdonald J. Dynamic soil-structure interaction issues of offshore wind turbines. Proc Int Conf Struct Dyn, EURODYN. 2014;2014:3611-3617.
- 31. Gazetas G. Foundation vibrations. Foundation Engineering Handbook. Chapman & Hall, New York. 1991;553-593.
- 32. Amar Bouzid D, Bhattacharya S, Otsmane L. Assessment of natural frequency of installed offshore wind turbines using nonlinear finite element model considering soil-monopile interaction. *J Rock Mech Geotech Eng.* 2018;10(2):333-346.
- 33. Arany L, Bhattacharya S, Macdonald JHG, Hogan SJ. Closed form solution of Eigen frequency of monopile supported offshore wind turbines in deeper waters incorporating stiffness of substructure and SSI. *Soil Dyn Earthq Eng.* 2016;83:18-32.
- 34. Bisoi S, Haldar S. Dynamic analysis of offshore wind turbine in clay considering soil-monopile-tower interaction. *Soil Dyn Earthq Eng.* 2014:63:19-35.
- 35. Jonkman J, Butterfield S, Musial W, Scott G. Definition of a 5-MW reference wind turbine for offshore system development. *Technical report: NREL/TP-500-38060, National Renewable Engergy Laboratory.* 2009;1-75.
- 36. Kaynia AM. Effect of kinematic interaction on seismic response of offshore wind turbines on monopiles. *Earthq Eng Struct Dyn.* 2021;50(3):777-790.
- 37. Pender MJ. Aseismic pile foundation design analysis. Bull New Zeal Natl Soc Earthq Eng. 1993;26(1):49-160.
- 38. Yang J, Gu XQ. Shear stiffness of granular material at small strains: does it depend on grain size? Geotechnique. 2013;63(2):165-179.
- 39. Seed H, Idriss I. Soil moduli and damping factors for dynmaic response analyses. Report: EERC 70-10. Earthquake Eng Res Center, Univ California, Berkeley. 1970;1-48
- 40. Hardin B, Drnevich V. Shear modulus and damping in soils: design equations and curves. Soil Mech Found Div. 1972;98(SM7):667-692.
- 41. Hardin B, Black W. Sand stiffness under various triaxial stresses. Soil Mech Found. 1996;92(2):27-42.
- 42. DNV-GL. Offshore Soil Mechanics and Geotechnical Engineering. DNVGL-RP-C212. 2017;1-184.
- 43. Verruijt A. Offshore Soil Mechanics. 2nd ed. Delft University of Technology; 2006.
- 44. ABAQUS. User's Manual, Version 6.14. Computer Software. Dassault Systèmes, Karlsson & Sorenson, Inc., 2022.
- 45. Zuo H, Bi K, Hao H. Dynamic analyses of operating offshore wind turbines including soil-structure interaction. Eng Struct. 2018;157:42-62.

- 46. Ali A, De Risi R, Sextos A. Seismic assessment of wind turbines: how crucial is rotor-nacelle-assembly numerical modeling? *Soil Dyn Earthq Eng.* 2021;141:106483.
- 47. Yin LL, Lo KH, Wang SS. Effects of blade pitch, rotor yaw, and wind-wave misalignment on a large offshore wind turbine dynamics in western Gulf of Mexico shallow water in 100-year return hurricane. *J Offshore Mech Arct Eng.* 2017;139(1):011901.
- 48. Zhang J, Yuan GK, Zhu S, Gu Q, Ke S, Lin J. Seismic analysis of 10 MW offshore wind turbine with large-diameter monopile in consideration of seabed liquefaction. *Energies*. 2022;15(7):2539.
- 49. Bhattacharya S, Nikitas G, Arany L, Nikitas N. Soil-structure interactions for offshore wind turbines. IET Eng Technol Ref. 2017;24(16):1-23.
- 50. Senanayake A, Manuel L, Gilbert RB. Estimating natural frequencies of monopile supported offshore wind turbines using alternative P-Y models. *Proc Annu Offshore Technol Conf.* 2017;6:4497-4507.
- 51. Skau KS, Jostad HP, Eiksund G, Sturm H. Modelling of soil-structure-interaction for flexible caissons for offshore wind turbines. *Ocean Eng.* 2019;171:273-285.
- 52. Sunday K, Brennan F. Influence of soil–structure modelling techniques on offshore wind turbine monopile structural response. *Wind Energy*. 2022;25(6):998-1012.
- 53. Yang S, Deng X, Yang J. Modeling of soil-pile-structure interaction for dynamic response of standalone wind turbines. *Renew Energy*. 2022;186(C):394-410. doi:10.1016/j.renene.2021.12.066
- 54. Dong R. Effective mass and damping of submerged structures. Report: UCRL-52342. 1978;1-78.
- 55. DNV-OS-J101. Design of Offshore Wind Turbines Structures. Offshore Standard, Det Norske Veritas. 2014;1-238.
- 56. Carswell W, Johansson J, Løvholt F, Arwade SR, DeGroot DJ. Dynamic mudline damping for offshore wind turbine monopiles. In: *Proceedings of the International Conference on Offshore Mechanics and Arctic Engineering—OMAE.* Vol 9A; 2014.
- 57. Jung S, Kim SR, Patil A, Hung LC. Effect of monopile foundation modeling on the structural response of a 5-MW offshore wind turbine tower. *Ocean Eng.* 2015;109:479-488.
- 58. Abed Y, Bouzid DA, Bhattacharya S, Aissa MH. Static impedance functions for monopiles supporting offshore wind turbines in nonhomogeneous soils-emphasis on soil/monopile interface characteristic. *Earthq Struct*. 2016;10(5):1143-1179.
- 59. Shadlou M, Bhattacharya S. Dynamic stiffness of monopiles supporting offshore wind turbine generators. *Soil Dyn Earthq Eng.* 2016;88:15-32
- 60. Ma H, Yang J, Chen L. Numerical analysis of the long-term performance of offshore wind turbines supported by monopiles. *Ocean Eng.* 2017:136(March):94-105.
- 61. TM L. Wind Energy Engineering: A Handbook for Onshore and Offshore Wind Turbines. 2nd ed. Elsevier, ISBN 978-0-12809451. 2017; p600.
- 62. Chopra AK. Dynamics of Structures. 3rd ed. Pearson/Prentice Hall. 2007; p 876.
- 63. Paz M, Kim YH. Structural Dynamics—Theory and Computation. 6th ed. Springer. 2019.
- 64. ASCE7-16. Minimum Design Loads for Buildings and Other Structures. American Society of Civil Engineer (ASCE) Standard. 2016.
- 65. EN1991-1 E8. Eurocode 8: Design of structure for earthquakeresistance Part 1: General rules, seismic actions and rules for buildings. *European Standard*. 2005.
- 66. Clough RW, Penzien J. Dynamics of Structures. Berkeley, Computers & Structures, Inc. USA; 1995.
- 67. Butt UA, Ishihara T. Seismic load evaluation of wind turbine support structures considering low structural damping and soil structure interaction. *Eur Wind Energy Conf Exhib 2012, EWEC 2012*. 2012;1:439-447.
- 68. Raju S. Finite Element Method (FEM) Model Verification and Validation for Bridges, Buildings and other Structures with Resensys Wireless SenSpot TM Sensors Measurements. Application notes, Resensys LLC. 2015; 1-6.
- 69. William FVI, Shin TW. The advanced p-y method for analyzing the behaviour of large diameter monopiles supporting offshore wind turbines. E3S Web Conf., 2nd International Conference on Energy Geotechnics (ICEGT). 2020;205:12008.
- 70. Karatzia X, Mylonakis G. Horizontal response of piles in inhomogeneous soil: simple analysis. *Proceedings of 2nd Int Conf Performance-Based, Des Earthq Geotech Eng*, Taormina, Italy, May, 2012;1117:1-16.
- 71. Abo-Khalil AG, Alyami S, Sayed K, Alhejji A. Dynamic modeling of wind turbines based on estimated wind speed under turbulent conditions. *Energies*. 2019;12(10):1907.

**How to cite this article:** Sah UK, Yang J. Importance of higher modes for dynamic soil structure interaction of monopile-supported offshore wind turbines. *Earthquake Engng Struct Dyn.* 2024;53:2006–2031.

monopile-supported offshore winhttps://doi.org/10.1002/eqe.4095